REPORT DOCUMENTATION PAGE

Form Approved OMB NO. 0704-0188

1. REPORT DATE (DD-MM-YYYY)	2. REPORT TYPE	3. DATES COVERED (From - To)
01-05-2015	Final Report	1-Jul-2009 - 30-Jun-2014

4. TITLE AND SUBTITLE
Final Report: Performance Limits of Non-Line-of-Sight Optical Communications

5a. CONTRACT NUMBER
W911NF-09-1-0293

5b. GRANT NUMBER

5c. PROGRAM ELEMENT NUMBER
611102

6. AUTHORS
Gang Chen

5d. PROJECT NUMBER

5e. TASK NUMBER

5f. WORK UNIT NUMBER

7. PERFORMING ORGANIZATION NAMES AND ADDRESSES
University of California - Riverside
200 University Office Building

Riverside, CA 92521 -0001

8. PERFORMING ORGANIZATION REPORT NUMBER

9. SPONSORING/MONITORING AGENCY NAME(S) AND ADDRESS (ES)
U.S. Army Research Office
P.O. Box 12211
Research Triangle Park, NC 27709-2211

10. SPONSOR/MONITOR'S ACRONYM(S)
ARO

11. SPONSOR/MONITOR'S REPORT NUMBER(S)
56047-NS.15

12. DISTRIBUTION AVAILIBILITY STATEMENT
Approved for Public Release; Distribution Unlimited

13. SUPPLEMENTARY NOTES
The views, opinions and/or findings contained in this report are those of the author(s) and should not contrued as an official Department of the Army position, policy or decision, unless so designated by other documentation.

14. ABSTRACT
Solar blind ultraviolet (UV) communication technology holds the promise of superior non-line-of-sight (NLOS) link connectivity through atmospheric scattering, and significantly relaxed tracking and pointing requirements. During the last Project, the research group at the University of California, Riverside, recently demonstrated these attributes, based on deep UV light emitting diodes (LEDs), solar blind filters, and high efficiency solar blind photo detectors. In this project, we address the main challenges towards optimizing the UV communication system performance. It covers channel modeling, channel capacity, advanced communication and network techniques, high

15. SUBJECT TERMS
Ultraviolet, Non-Line-of-Sight, scattering optical channel, communication performance, network MAC.

16. SECURITY CLASSIFICATION OF:			17. LIMITATION OF ABSTRACT	15. NUMBER OF PAGES	19a. NAME OF RESPONSIBLE PERSON
a. REPORT	b. ABSTRACT	c. THIS PAGE			Gang Chen
UU	UU	UU	UU		19b. TELEPHONE NUMBER 951-827-2953

Report Title

Final Report: Performance Limits of Non-Line-of-Sight Optical Communications

ABSTRACT

Solar blind ultraviolet (UV) communication technology holds the promise of superior non-line-of-sight (NLOS) link connectivity through atmospheric scattering, and significantly relaxed tracking and pointing requirements. During the last Project, the research group at the University of California, Riverside, recently demonstrated these attributes, based on deep UV light emitting diodes (LEDs), solar blind filters, and high efficiency solar blind photo detectors. In this project, we address the main challenges towards optimizing the UV communication system performance. It covers channel modeling, channel capacity, advanced communication and network techniques, high sensitive transceiver design and different system tradeoffs. First, both integrated analytical and Monte Carlo UV channel models are developed to simulate the channel impulse response and pass loss. Second, UV LEDs based and UV laser based channel test platforms are built to experimentally study UV channel characteristics and validate the models. Aware of the huge pass loss property of a UV signal, it is hard to synchronize the UV signal frame. We integrate Universal Software Radio Peripheral (USRP) into UV communication system and employ GPS as synchronized signal to get better communication performance. Based on NLOS communication link geometry and UV signal interaction with the atmosphere, we develop two analytical channel models that describe the path loss in an integral form and closed-form respectively. Utilizing curve-fitting with field measurements, an easy-to-use empirical model is further developed. The results are then applied to study performance of a NLOS UV network, from outage probability to transmission throughput and network connectivity in a multi-user interference environment. For the UV network, we develop a novel contention-based MAC protocol (UVOC-MAC) that inherently accounts for the UV PHY layer and fully exploits multi-fold spatial reuse opportunities. We further develop an efficient neighbor discovery protocols by accounting for the varying channel qualities along different scattering directions.

Enter List of papers submitted or published that acknowledge ARO support from the start of the project to the date of this printing. List the papers, including journal references, in the following categories:

(a) Papers published in peer-reviewed journals (N/A for none)

Received	Paper
05/01/2014 10.00	H. Ding, G. Chen, Z. Xu, B.M. Sadler. Channel modelling and performance of non-line-of-sight ultraviolet scattering communications, IET Communications, (06 2012): 0. doi: 10.1049/iet-com.2011.0026
05/01/2014 12.00	Leijie Wang, Yiyang Li, Zhengyuan Xu. On connectivity of wireless ultraviolet networks, Journal of the Optical Society of America A, (09 2011): 0. doi: 10.1364/JOSAA.28.001970
TOTAL:	**2**

Number of Papers published in peer-reviewed journals:

(b) Papers published in non-peer-reviewed journals (N/A for none)

Received	Paper
TOTAL:	

Number of Papers published in non peer-reviewed journals:

(c) Presentations

Number of Presentations: 0.00

Non Peer-Reviewed Conference Proceeding publications (other than abstracts):

Received	Paper

TOTAL:

Number of Non Peer-Reviewed Conference Proceeding publications (other than abstracts):

Peer-Reviewed Conference Proceeding publications (other than abstracts):

Received		Paper
05/01/2014	13.00	Leijie Wang, Yiyang Li, Zhengyuan Xu, Srikanth V. Krishnamurthy. A novel neighbor discovery protocol for ultraviolet wireless networks, the 14th ACM international conference. 30-OCT-11, Miami, Florida, USA. : ,
08/31/2011	1.00	H. Ding, G. Chen, A. K. Majumdar, B. M. Sadler, Z. Xu. Turbulence modeling for non-line-of-sight ultraviolet scattering channels, SPIE Defense, Security, and Sensing. 24-APR-11, . : ,
08/31/2011	2.00	Leijie Wang, Yiyang Li, Zhengyuan Xu, Brian M. Sadler. Wireless ultraviolet network models and performance in noncoplanar geometry, EEE Globecom 2010 Workshop on Optical Wireless Communications (OWC 2010). , . : ,
08/31/2011	3.00	Qunfeng He, Zhengyuan Xu, Brian M. Sadler. Non-line-of-sight Serial Relayed Link for OpticalWireless Communications, 2010 IEEE Military Communications Conference. 30-OCT-10, . : ,
08/31/2011	4.00	Yiyang Li, Jianxia Ning, Zhengyuan Xu, Srikanth V. Krishnamurthy, Gang Chen. UVOC-MAC: A MAC Protocol for Outdoor Ultraviolet Networks, 18th IEEE International Conference on Network Protocols (ICNP 2010). 04-OCT-10, . : ,
08/31/2011	5.00	Leijie Wang, Qunfeng He, Zhengyuan Xu, Brian M. Sadler. Performance of non-line-of-sight ultraviolet communication receiver in ISI channel, roc. of SPIE Photonics and Optics – Free Space Laser Communications X. 31-JUL-10, . : ,
08/31/2011	6.00	Gang Chen, Zhengyuan Xu, Brian M. Sadler. Experimental demonstration of non-line-of-sight ultravioletcommunication channel characteristics, SPIE Photonics and Optics – Free Space Laser Communications X. 10-AUG-10, . : ,
TOTAL:	**7**	

Number of Peer-Reviewed Conference Proceeding publications (other than abstracts):

(d) Manuscripts

Received		Paper
08/31/2011	7.00	Yiyang Li, Leijie Wang, Zhengyuan Xu, Srikanth V. Krishnamurthy. Neighbor Discovery for Ultraviolet Ad Hoc Networks, IEEE Journal on Selected Areas in Communications (08 2011)
08/31/2011	8.00	Leijie Wang, Zhengyuan Xu, and Brian M. Sadler. An approximate closed-form link loss model for non-line-of-sightultraviolet communication in non-coplanar geometry, Optics Letters (02 2011)
TOTAL:		**2**

Number of Manuscripts:

Books

Received	Book
TOTAL:	

Received	Book Chapter
TOTAL:	

Patents Submitted

Patents Awarded

Awards

Best paper award?H. Ding, G. Chen, Z. Xu, and B. M. Sadler, “Characterization and Modeling of Non-Line-of-Sight Ultraviolet Scattering Communication Channels,” 7th IEEE & IET International Symposium on Communication Systems, Networks and Digital Signal Processing: 2nd Colloquium on Optical Wireless Communications, Newcastle, UK, July 21-23, 2010.

Graduate Students

NAME	PERCENT_SUPPORTED	Discipline
Yiyang Li	0.80	
Leijie Wang	0.80	
Hiapeng Ding	1.00	
Linchao Liao	1.00	
Qian Gao	0.20	
Zening Li	0.20	
Samuel Ibarra	0.20	
FTE Equivalent:	**4.20**	
Total Number:	**7**	

Names of Post Doctorates

NAME	PERCENT_SUPPORTED
FTE Equivalent:	
Total Number:	

Names of Faculty Supported

NAME	PERCENT_SUPPORTED	National Academy Member
Gang Chen	0.50	No
FTE Equivalent:	**0.50**	
Total Number:	**1**	

Names of Under Graduate students supported

NAME	PERCENT_SUPPORTED
FTE Equivalent:	
Total Number:	

Student Metrics

This section only applies to graduating undergraduates supported by this agreement in this reporting period

The number of undergraduates funded by this agreement who graduated during this period: 0.00

The number of undergraduates funded by this agreement who graduated during this period with a degree in science, mathematics, engineering, or technology fields:..... 0.00

The number of undergraduates funded by your agreement who graduated during this period and will continue to pursue a graduate or Ph.D. degree in science, mathematics, engineering, or technology fields:..... 0.00

Number of graduating undergraduates who achieved a 3.5 GPA to 4.0 (4.0 max scale):..... 0.00

Number of graduating undergraduates funded by a DoD funded Center of Excellence grant for Education, Research and Engineering:..... 0.00

The number of undergraduates funded by your agreement who graduated during this period and intend to work for the Department of Defense 0.00

The number of undergraduates funded by your agreement who graduated during this period and will receive scholarships or fellowships for further studies in science, mathematics, engineering or technology fields: 0.00

Names of Personnel receiving masters degrees

NAME
Samuel Ibarra
Total Number: 1

Names of personnel receiving PHDs

NAME
Yiyang Li
Leijie Wang
Haipeng Ding
Qian Gao
Total Number: 4

Names of other research staff

NAME	PERCENT_SUPPORTED
FTE Equivalent:	
Total Number:	

Sub Contractors (DD882)

Inventions (DD882)

Scientific Progress

Technology Transfer

Performance Limits of Non-Line-of-Sight Optical Communications Final Report

Gang Chen, University of California, Riverside, CA 92521
gachen@ee.ucr.edu, 951-827-2953

Project Information

Proposal Number:	56047NS
Agreement Number:	W911NF-09-1-0293
Proposal Title:	Performance Limits of Non-Line-of-Sight Optical Communications
Project Period:	1 July 2009 – 30 June 2014

Abstract

Solar blind ultraviolet (UV) communication technology holds the promise of superior non-line-of-sight (NLOS) link connectivity through atmospheric scattering, and significantly relaxed tracking and pointing requirements. During the last Project, the research group at the University of California, Riverside, recently demonstrated these attributes, based on deep UV light emitting diodes (LEDs), solar blind filters, and high efficiency solar blind photo detectors. In this project, we address the main challenges towards optimizing the UV communication system performance. It covers channel modeling, channel capacity, advanced communication and network techniques, high sensitive transceiver design and different system tradeoffs. First, both integrated analytical and Monte Carlo UV channel models are developed to simulate the channel impulse response and pass loss. Second, UV LEDs based and UV laser based channel test platforms are built to experimentally study UV channel characteristics and validate the models. Aware of the huge pass loss property of a UV signal, it is hard to synchronize the UV signal frame. We integrate Universal Software Radio Peripheral (USRP) into UV communication system and employ GPS as synchronized signal to get better communication performance. Based on NLOS communication link geometry and UV signal interaction with the atmosphere, we develop two analytical channel models that describe the path loss in an integral form and closed-form respectively. Utilizing curve-fitting with field measurements, an easy-to-use empirical model is further developed. The results are then applied to study performance of a NLOS UV network, from outage probability to transmission throughput and network connectivity in a multi-user interference environment. For the UV network, we develop a novel contention-based MAC protocol (UVOC-MAC) that inherently accounts for the UV PHY layer and fully exploits multi-fold spatial reuse opportunities. We further develop an efficient neighbor discovery protocols by accounting for the varying channel qualities along different scattering directions.

Table of Contents

Acknowledgments

We gratefully acknowledge the support of Dr. Brian M. Sadler in the Army Research Lab (ARL) for his various forms of support, input and feedback on this research. We are thankful to Dr. Robert J. Drost in ARL in modeling the UV channel and tests. We also acknowledge Professor Srikanth V. Krishnamurthy's insightful guidance on UV network protocol design. At last, I would like to acknowledge all the members of our research group, Dr. Daniel Xu, Dr. Haipeng Ding, Dr. Qunfeng He, Dr. Yiyang Li, Dr. Leijie Wang and Linchao Liao for their hard work.

1. Introduction

As an optical technology, UV offers another frequency channel that is orthogonal to radio frequency (RF), microwave, or infrared. The regulated radio spectrum is becoming increasingly congested, but bandwidth demand is growing rapidly. Optical wireless provides an attractive way to circumvent bandwidth limitations as a complement to RF wireless. The available optical bandwidth is huge and unregulated. The optical system can share the governance of a network with RF in a hybrid optical/RF network. With the unique scattering and absorption properties of ultraviolet (UV) waves propagating through an atmospheric channel, the UV spectrum is ideal for diverse short-range communication environments, including line-of-sight (LOS) and non-line-of-sight (NLOS) communication channels. By operating in the solar blind band, a receiver of low dark noise can exploit the very low solar background to achieve excellent a signal-to-noise ratio (SNR) and quantum noise limited photon-counting detection. Meanwhile, due to the huge and unlicensed UV spectrum, high data rate services are potentially deliverable at very low cost. But these benefits can be realized only with technological advances in both miniaturized low-power solid-state UV devices and advanced UV communication technology.

First of all, over the whole UV spectrum (4~400nm), the UV-C (200~280nm) or “deep UV” band is solar blind at ground level due to ozone absorption in the upper atmosphere. By operating in this band, a ground-based photodetector, if low dark noise, can exploit the negligible background radiation and approach quantum noise limited photon-counting detection. This characteristic encourages deployment of wide field-of-view (FOV) receivers that greatly increase SNR. Second, a high degree of relatively angle-independent scattering occurs when UV waves transverse the atmosphere, creating tremendous communication paths from a source to a destination. Consequently, NLOS communication is enabled. It thus relaxes stringent pointing, acquisition and tracking (PAT) requirements, even in a LOS scenario. This phenomenon makes UV suitable for different link set-ups. Third, due to high attenuation by the atmosphere, signal beyond the extinction range (on the order of kilometers) can hardly be detected, a desirable feature for short-range secure communications and spectrum reuse.

Ultraviolet communication has received increased attention due to unique channel characteristics. A series of relevant UV communication studies have been conducted since the 1960s in academia, government agencies and defense industry. However, those communication systems were based on bulky and power-hungry flashtubes/lamps/lasers as light sources. Also they targeted long-range communications. Recent technologies in low-cost, small-size, low-power, high-reliability, and high-bandwidth deep UV LEDs and avalanche photodiodes (APDs) have motivated extensive research in low-power short-range UV communications. State-of-the-art commercial deep UV LEDs have become available. These include deep UV LEDs at 247~365nm peak wavelengths and with a 20nm spectral

width. Improvements on power output, efficiency and reliability are promising and being undertaken.

To develop an effective UV communication transceiver that can operate under exposure to solar radiation, it is crucial to have solar-blind UV detectors and filters with high sensitivity, gain, and out-of-band rejection. These requirements make PMTs and APDs suitable candidates. Commercial off-the-shelf UV PMTs (Hamamatsu or PerkinElmer) attain high multiplication gains of 10^5 ~10^7, high responsivity of 62A/W, large detection area of few cm^2, reasonable quantum efficiency of 15%, low dark count rate of a few hertz, low dark current of a fraction of 1nA/cm^2, and response time typically on the order of 20ns. For solar blind applications, PMTs are typically combined with solar-blind filters resulting in an enhanced out-of-band rejection ratio of about 10^8. These features enable PMTs to detect very weak signals in a photon counting mode even in the presence of high level background radiation, down to single photon resolution. However, PMTs tend to be fragile, bulky, costly, sensitive to magnetic interference, and need to be integrated with external filters. These attributes prohibit low-cost and compact designs. Accordingly, research in solid-state solar-blind deep UV APDs is rapidly growing. Emerging devices are potentially small and low-cost, and can be intrinsically made solar blind. Thus far, the GaN-based research has resulted in responsivity of 0.15A/W, gain of 10^4, and dark current of 100nA/cm^2 and single photon counting. The Wireless Information Technology Lab directed by the PI at the University of California, Riverside (UCR) is pleased to be part of the contributors, focusing on experimental and analytical study of solar-blind UV communications.

From an application perspective, UV technology is suitable for both commercial and military applications. Examples includes dedicated building-to-building or “last mile” wireless communication, sensing of explosive/chemical/biological agents, sensing of missile flame/fire, atmospheric characterization (wind speed, temperature, particle density, pollutant, etc.), distributed sensor networks, aircraft landing aid , unattended ground sensor networks and small unit communications in urban terrain environments . Other applications that have not been envisioned yet may also be possible. For conditions under which low-power consumption, low-cost implementation, security and less restrictive pointing are essential, while range and bandwidth requirements are modest, the UV technology is an excellent candidate. The NLOS operability is expected to apply to scenarios where direct sight is blocked or visibility is reduced by buildings, mountains, trees, fog, or smoke. Even in LOS conditions, low background noise and relaxed pointing requirements make UV more advantageous in system performance than its competitors.

Technical Objectives

To meet the application needs for short-range communications, this project build upon our existing research to thoroughly study fundamental communication performance limits under atmospheric UV channels that in turn prompt associated performance optimization techniques

for range up to hundreds of meters using low power LEDs. The following objectives appear to be both scientifically and practically important:

(1) Characterize communication links (LOS and NLOS) and model channels using non-parametric approaches based on wave propagation theory as well as stochastic photon detection theory, and parametric approaches for goodness-of-fit analysis.

(2) Study atmospheric UV channel capacity across the Poisson regime and Gaussian regime and bridge an existing gap.

(3) Perform communication performance tradeoff studies in data rate, communication range, power budget, SNR and bit-error-rate (BER) based on waveform processing or photon counting. Then reveal performance limits that will serve as guidelines for optimization of communication performance.

(4) Develop advanced communication techniques in appropriate coding, adaptive modulation and diversity to achieve optimal detection in the presence of significant channel distortions, interference, and noise.

(5) Test and analyze the proposed models and techniques both analytically using theoretical tools and experimentally via measurement campaigns and simulations.

(6) Develop Media Access Control (MAC) protocols to optimize the UV network performance.

2. UV channel modeling and verification

The most significant part of communication system design is the end-to-end channel model. A good channel model is a prime for higher layer design and it also enable accurate performance prediction and the comparison of different communication approaches. Therefore, extensive research work have been performed on the NLOS UV channel modeling, not only experimentally, but also theoretically. These channel models mainly give out a way to estimate the NLOS link path loss and/or NLOS channel r impulse response function (IRF) given the communication system geometry, roughly including separation distance, transmitter pointing angle, receiver pointing angle, transmitted beam angle and receiver field of view (FOV). Next, we are going to briefly summary our work about UV NLOS channel model.

- **Single Scattering Model**

2.1.1 *Analytical Single Scattering Model*

Fig. 2.1 depicts the basic system geometry in the scenario of single scattering channel. We denote the full-width divergence of the transmitter beam as φ_1, the field-of-view (FOV) angle of the receiver as φ_2, the transmitter elevation angle as Θ_1, the receiver elevation angle as Θ_2, the baseline separation of the transmitter and receiver as r, and the distances from the common volume V to the transmitter and receiver as r_1 and r_2, respectively.

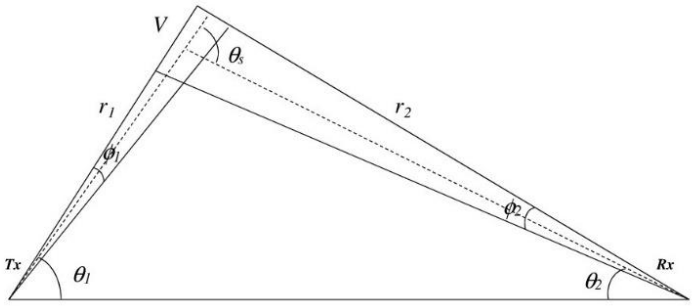

Figure 2.1: Single scattering system geometry

An analytical channel model was firstly proposed in [1]. Assuming the common volume is small and with scattering phase function in [2], the coplanar link path loss can be approximated obtained from [1] with the system geometry as variables:

$$L \approx \frac{96 r \sin\Theta_1 \sin^2\Theta_2 \left(1-\cos\frac{\varphi_1}{2}\right) \exp\left[\frac{k_e r(\sin\Theta_1+\sin\Theta_2)}{\sin\Theta_s}\right]}{k_s P(\mu) A_r \varphi_1^2 \varphi_2 \sin\Theta_s (12\sin^2\Theta_2+\varphi_2^2\sin^2\Theta_1)} \qquad (1)$$

Where, $P(\mu)$ is the scattering phase function and this phase function is modeled as a weighted sum of the Rayleigh (molecular) and Mie (aerosol) scattering phase functions based on the corresponding scattering coefficients.

$$P(\mu)=\frac{k_s^{Ray}}{k_s}p^{Ray}(\mu)+\frac{k_s^{Mie}}{k_s}p^{Mie}(\mu) \qquad (2)$$

Where $\mu=\cos(\Theta_s)$ is defined from the scattering angle Θ_s. The two phase function follows a generalized Rayleigh and a generalized Henyey-Greenstein function, respectively, which is given by

$$p^{Ray}(\mu)=\frac{3[1+3\gamma+(1-\gamma)\mu^2]}{16\pi(1+2\gamma)} \qquad (3)$$

$$p^{Mie}(\mu)=\frac{1-g^2}{4\pi}\left[\frac{1}{(1+g^2-2g\mu)^{3/2}}+f\frac{0.5(3\mu^2)-1}{(1+g^2)^{3/2}}\right] \quad (4)$$

Where γ, g, and f are model parameters.

The resulting path-loss predictions for various coplanar pointing directions and ranges are compared with corresponding path-loss measurements made using an LED-based test system, demonstrating reasonable agreement between theory and experiment.

Besides, we also develop a BER expression from path loss L. For direct detection by an ideal receiver, the BER under optimum detection of on–off keying signals is given by

$$BER=0.5\exp\left(-\frac{P_t\eta_f\eta_f\lambda}{LRhc}\right) \qquad (5)$$

Which involves several system parameters, such as transmitted power P_t, filter transmission rate η_f, and data rate R.

Compared to the widely adopted yet complex single scattering channel model, this proposed model is significantly simplified by means of a closed-form expression for tractable analysis.

2.1.2 *Parametric Single Scattering Model*

To further simplify the channel model and quickly estimate the channel path loss, [3] presents a parametric channel model by modeling the channel impulse response function (IRF) with a gamma function as well as its variants to better fit the prediction by a widely adopted analytical single scattering model. Normalized mean square fitting error is adopted to validate our parametric model. Path losses and channel bandwidths are subsequently studied under different geometrical link configurations.

It is shown that the IRF resulting from the evaluation of the single-scattering model can be approximated by a function of the form

$$h_{\Gamma} = \frac{Cu^{-v}}{\Gamma(v)} t^{v-1} e^{-t/u} \qquad (6)$$

or of the form

$$h_{L}(t) = \frac{Cu^{-v}}{\Gamma(v)} t^{v-1} e^{-t/u} \sum_{i=0}^{N} c_i L_i(t) \qquad (7)$$

Where $\Gamma(\cdot)$ is the gamma function, $L_i(\cdot)$ is the ith order Laguerre polynomial, and u, v, C, and the c_i are scalar parameters.

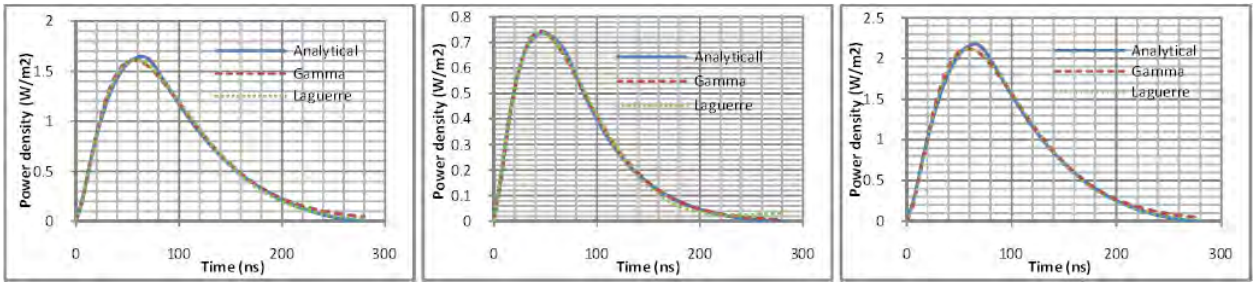

Figure 2.2: IRF comparison of three model

This proposed model is compared with analytical and Laguerre model (Fig. 2.2) and it can be observed that over a large range of temporal delay spread, the goodness-of-fit test is satisfactory, although there are clearly slight mismatches. Based on simulation results, we also find the mean-square-errors (MSEs) for two parametric models: 0.0003 for gamma fitting, and 0.00025 for modulated gamma fitting. Two models thus yield low MSEs.

Not only IRF, some sanity check are also done for this model. Based on different link geometry, we can see that received energy is insensitive to Θ_1 and β_2, but sensitive to Θ_2 and β_1. Therefore, we conclude that we can apply a wide FOV detector for system design regardless of transmitter's beam width.

Even if we note that the proposed forms can fail to well approximate the IRF when multiple scattering is significant, as will be discussed in the next subsection. Nevertheless, when single scattering is dominant, these parametric models can provide a means for analysis or rapid evaluation in a real-world system, possibly using tabulated fitting parameters.

- **Monte Carlo based multiple scattering model**

2.2.1 *Initial Monte Carlo*

Aware that the importance of multiple scattering, we extend our work to multiple scattering channel modeling. Fig. 2.3 illustrates the typical multiple scattering system geometry.

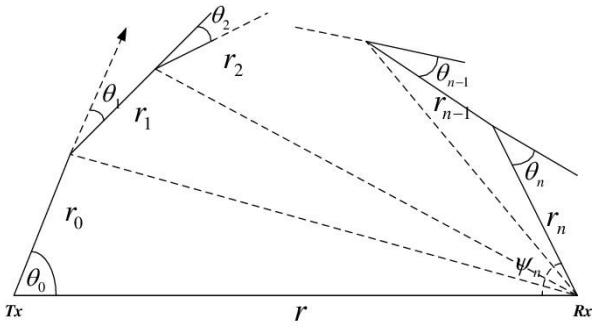

Figure 2.3: Non-coplanar system geometry

Assuming there are n times of scattering, one n time NLOS path is comprised of 2n segments, including n paths from the transmitting point to the scattering centers and n paths from scattering centers to the Rx. Given each scattering is self-governed, and the distances and angles for different scattering events are dependent on previous quantities. Therefore, on each segment, the photon's propagation is assumed to follow the law of single scattering until it reaches the next scattering center or arrives at the receiver. Following this theory, [6] proposes a Monte Carlo based multiple scattering channel model. The procedure is repeated for many photons independently. Fig. 2.4 shows the flow chart of our Monte Carlo photon tracing model.

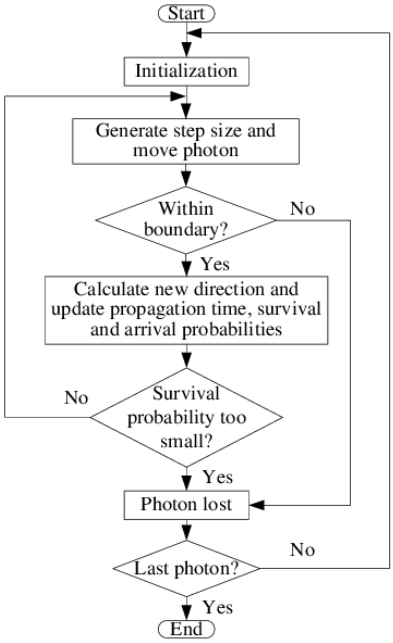

Figure 2.4: Monte Carlo simulation flowchart for channel modeling.

In this project, the comparisons of IRF predictions from single-scatter modelling and multiple-scattering modelling, as well as experimental measurements, are provided. Some path loss of particular system geometry have been compared for single scattering model,

multiple scattering model and field test results. The single scattering channel model was shown to typically underestimate the scattering effects, resulting in less accurate predictions. For example, Fig. 2.5 shows the impulse response from our photon tracing simulation. Also shown for comparison is a curve from a single scattering impulse response model, that assumes a single scattering event per photon, given by Eq. (3.13a) in Luettgen's paper [15] .It is observed that the impulse response predicted by the single scattering model has smaller temporal spread and area than the proposed multiple scattering model. In this scenario, accounting for multiple scattering events per photon reveals that more photons arrive at the detector, with more delay, than predicted with a single scattering model.

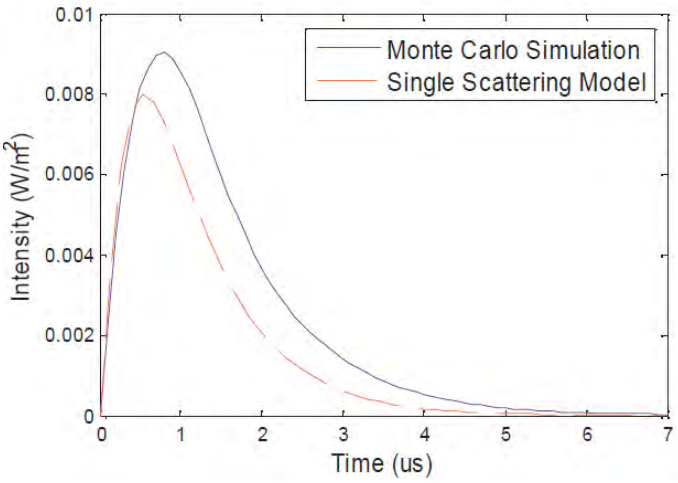

Figure 2.5: Simulated impulse response under single and multiple scattering assumptions

Fig. 2.6 indicate that our Monte Carlo method can provide a good prediction for experimental NLOS UV link performance, even with some mismatch in the atmospheric model parameters. We also observe that the single scattering model generally overestimates path loss.

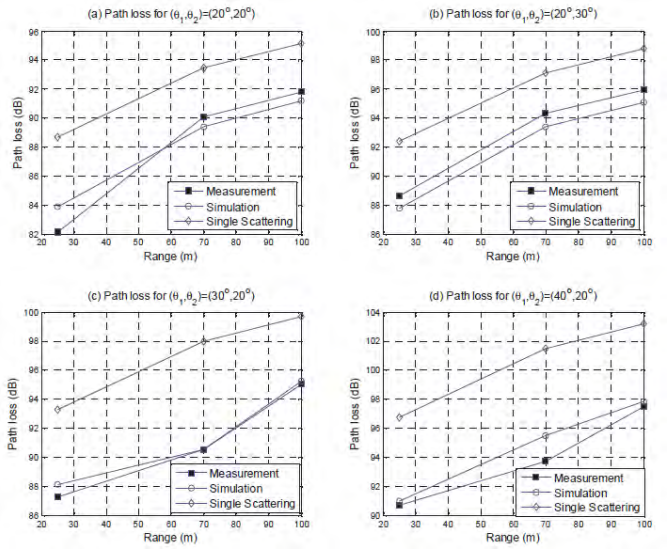

Figure. 2.6: Comparison of Monte Carlo multiple scattering path loss prediction, single scattering model prediction, and measurements.

2.2.2 *Monte Carlo Further Analysis*

After previous analysis, a more comprehensive comparison of single-scatter modelling, multiple scatter (Monte Carlo) modelling, and experimentally collected data for coplanar geometries is provided in [7]. This work also re-examines the Gamma function IRF model, showing a good fit to Monte Carlo results for particular system configurations.

Simulations explore path-loss and communication-bandwidth (as determined from predicted IRFs) trends as the elevation angles, transmitter beam width, receiver FOV, and wavelength are varied. For example, Fig. 2.7 illustrates range-dependent path loss: (a) varying Θ_1, (b) varying Θ_2, (c) varying φ_1, and (d) varying φ_2. Note that path loss is very sensitive to the angles when they are small. In particular, path loss has a high dependence on the Rx FOV φ_2. A wider Rx FOV yields lower path loss as the Rx is able to collect more scattered photons.

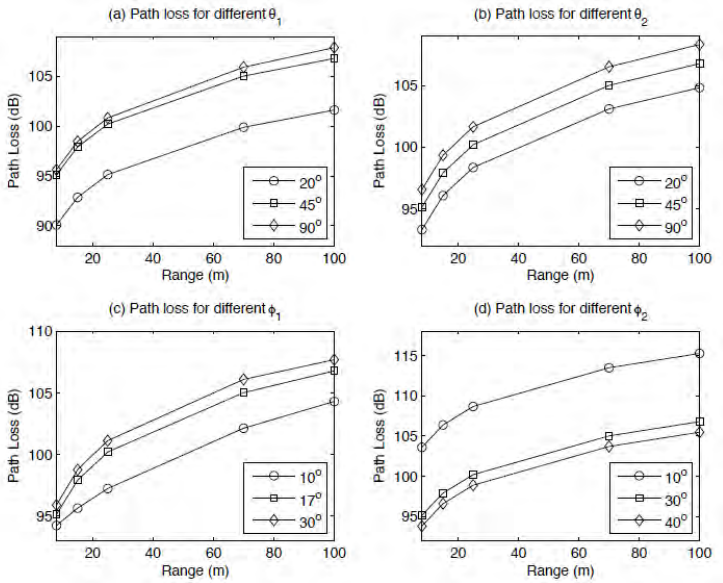

Figure 2.7: Predicted path loss for different optical geometries

In Fig. 2.8, we plot predicted range-dependent channel bandwidth as a function of the system geometry. Path loss naturally increases as the range increases, and the bandwidth shows significantly large fluctuation as a function of the elevation angles. Generally, channel bandwidth will degrade as the elevation angles, beam width or FOV angle increase. Thus, while wide Rx FOV is desirable to combat path loss, it also constrains the bandwidth due to the increased impulse response duration, leading to a fundamental system tradeoff between path loss and achievable rate.

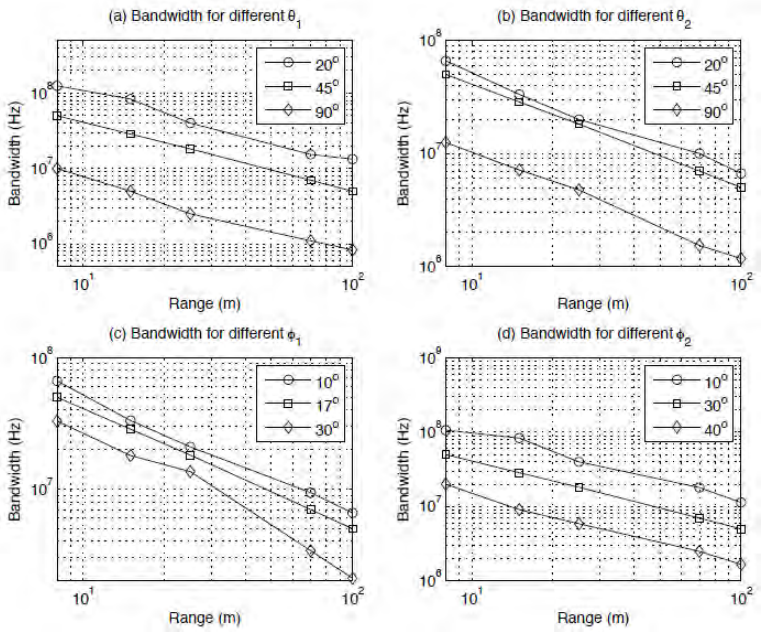

Figure 2.8: Predicted channel bandwidth for different optical geometries

In this work, we also consider the impact of optical wavelength on path loss. Fig. 2.9 shows path loss for wavelengths in [230, 310] nm at a range of r=70m, for three different pairs of Tx and Rx elevation angles.

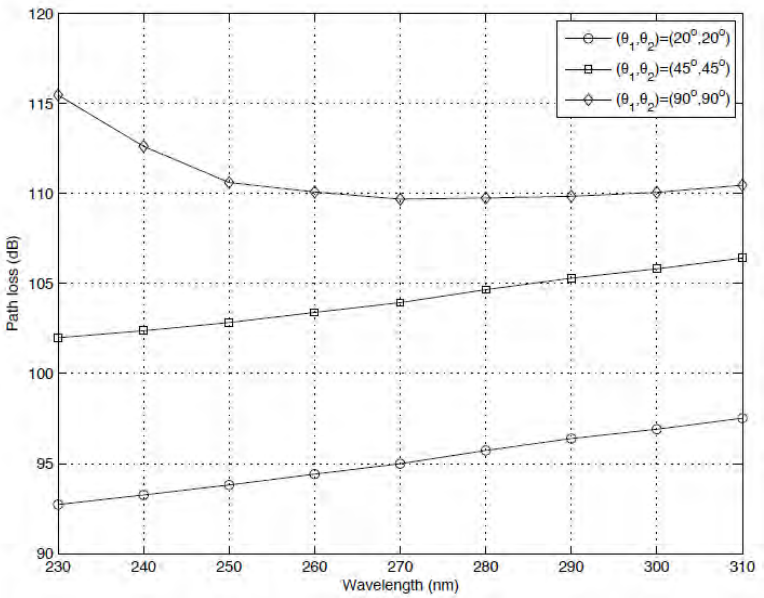

Figure 2.9: Predicted path loss dependence on wavelength, at a range of r = 70m.

For $(\Theta_1,\Theta_2)=(90^\circ,90^\circ)$, path loss decreases until 270nm, with a slight increase thereafter. Absorption loss may dominate scattering loss for shorter wavelength because of the larger absorption coefficient and long propagation distance, much larger than r. As the wavelength increases, the absorption loss decreases as reflected in the decreasing absorption coefficient, and scattering loss may become dominant. This explains the slightly increased path loss at longer wavelengths. For the smaller elevation angles, path loss increases slowly with increasing wavelength λ, at a rate proportional to $\lambda^{3.86}$ according to the slopes of the two lower curves in the figure. In this scenario, scattering loss dominates absorption loss, and the scattering loss increases as the wavelength increases. It is therefore desirable to use a shorter wavelength for short range communication when the elevation angles are not very large. In practice, however, optical devices may have lower efficiencies at shorter wavelengths, and this may offset any gain due to increased scattering. Considering typical solar blind operation of a communication system, about a 2dB gain is achieved going from 280nm to 250nm (according to the two lower curves in Fig. 2.9). A much more pronounced impact is observed from the optical geometry. A roughly 20dB gain is obtained when the elevation angles decrease from $(45^\circ,45^\circ)$ to $(20^\circ,20^\circ)$. We note that these trends may change significantly at longer ranges when absorption loss begins to dominate.

2.2.3 *Comprehensible Analysis*

What's more, a kind of analytical multiple scattering path loss model has been developed in [8]. In this method, integration is performed by sampling the possible paths uniformly, as opposed to basing the sampling distribution on realizations of transmission angles, propagation distances, and scattering angles.

In [16], we comprehensively analyze all kinds of NLOS UV channel modeling by comparing their predictions to field test results. Also we studied the the practical achievable data rate from two aspects. First we examine the channel 3 dB bandwidth from the simulated impulse response, then we investigate the data rate which is determined by the transmitted power, desired BER and link path loss. We aim to find out the fundamental determinant for the achievable data rate. Corresponding result show us that NLOS UV link is power limited based on current system parameters, instead of bandwidth limited. In addition to short range, this paper firstly considered the long distance scenario. For long range communication links, we examine both path loss and power requirement for different geometries at a range up to 5 kilometers. Our results shows that extra high path loss and high power requirement may be generated for large pointing angles at long ranges, while large FOV are enable to improve such conditions.

- **Non-coplanar Single Scattering Model**

Various path loss models have been developed for solar blind non-line-of-sight UV communication links under an assumption of coplanar source beam axis and receiver pointing direction. However, few work is related to non-coplanar path loss model. Thus, this trigged us to extend an existing single-scattering coplanar analytical model to non-coplanar geometry. In [4], a model is derived as a function of geometric parameters and atmospheric characteristics. Its behavior is numerically studied in different non-coplanar geometric settings.

We further extends an existing single-scattering coplanar analytical model to non-coplanar geometry by using a spherical coordinate system with the transmitter at the origin. Figure 2.10 demonstrates the typical system geometry of non-coplanar. Building on Fig. 2.10, we add one more parameter, off-axis angles from Tx to Rx.

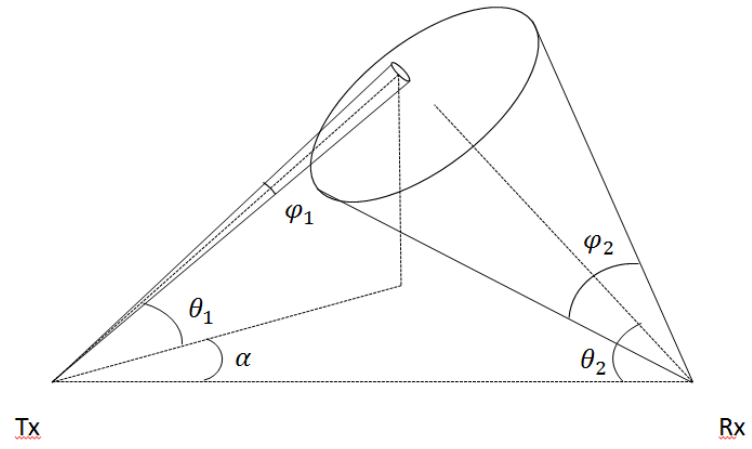

Figure 2.10: Non-coplanar system geometry

The path loss of different system geometries were also studied by applying this model as shown in Fig. 2.11.

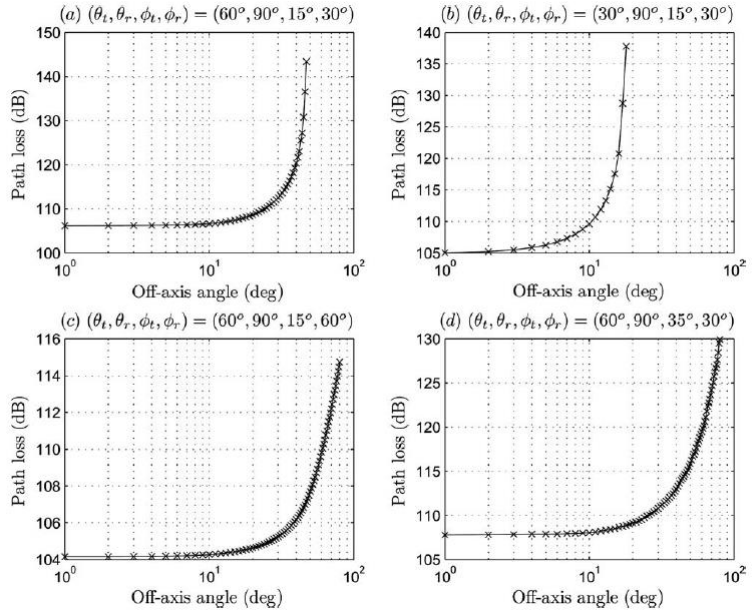

Figure 2.11: Path loss per cm2 versus off-axis angle

But in [4], we only consider the case that receiver's pointing angle is always vertical. Thus, an approximate closed-form link loss model for arbitrary pointing angles in non-coplanar geometry is develop in [5]. The performance of this model is also verified in Fig. 2.12.

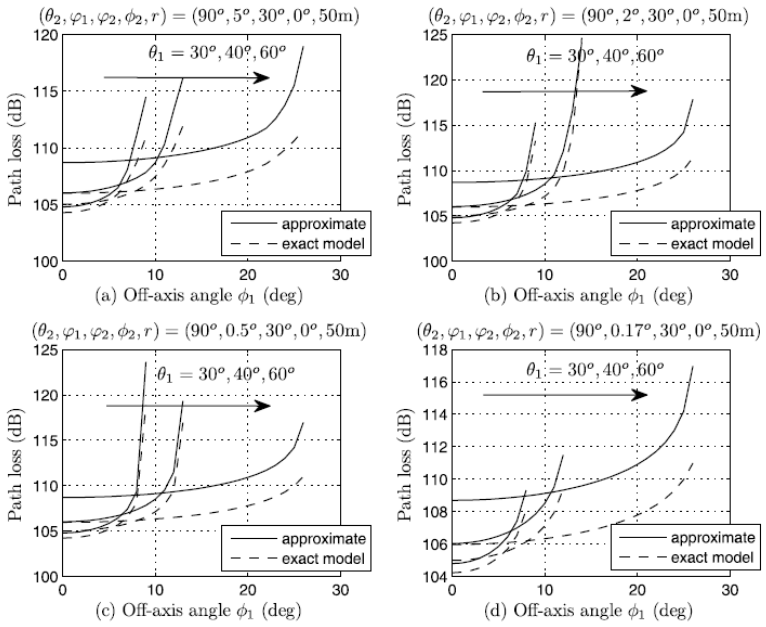

Figure 2.12: Comparison of proposed model and model

Fig. 2.12 compares path loss versus Φ_1 for two models: (i) our proposed closed-form approximation for arbitrary non-coplanar geometry, and (ii) the integral based exact model for Rx vertical pointing. The four subplots correspond to φ_1 equal to 5°,2°,0.5°,0.17°, while $(\Theta_2,\varphi_2,\Phi_2,r)=(90^\circ,30^\circ,0^\circ,50m)$. In each subplot, the three curves are parameterized by Θ_1 for 30°,40°, and 60°. We observe good model agreement when φ_1 and Θ_1 are both small. As φ_1 increases, the shape of the beam and FOV intersection becomes more asymmetric and skewed. This results in underestimation of the common volume in our approximation, and the path loss is overestimated. This becomes more evident as the intersection diminishes, with a sharp climb in path loss as φ_1 grows. The approximation error also increases as $|\Theta_1+\Theta_2+90^\circ|$ grows, with underestimation of the intersection height and common volume, resulting in overestimation of the path loss. In summary, this simple closed-form expression for single-scattering path loss in non-coplanar geometry that is much easier to evaluate than integral based or Monte Carlo models, and the approximation is best when Θ_1 and φ_1 are relatively small.

- **Channel experiments**

To validate the channel models, we have experimentally measured both path loss and impulse response, by employing UV LED array and UV laser, respectively. All the experimental results are based on the solar blind UV communication test-bed as depicted in Fig. 2.13.

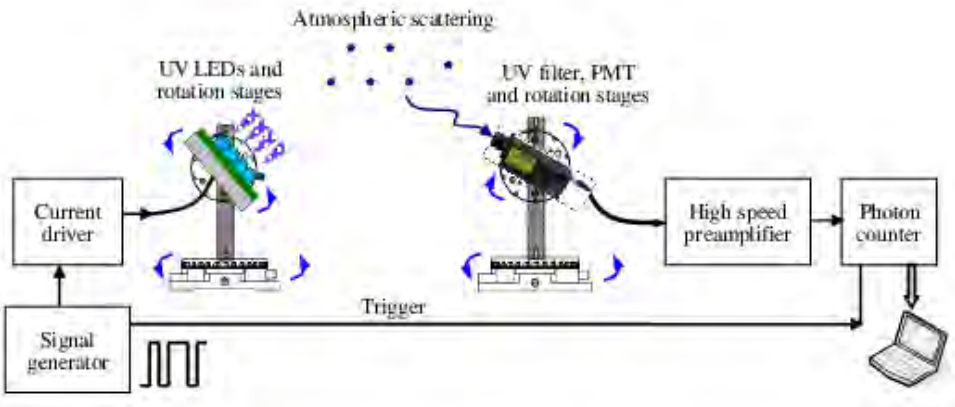

Figure 2.13: LED based NLOS path loss measurement system diagram.

2.4.1 LED based path loss measurements

By using a solar blind UV path loss experimental test-bed at 260 nm wavelength, as shown in Fig. 2.13, [9] firstly report the initial experiment results, including solar irradiance and signal

count distributions, path loss for some particular system geometries, and system BER performance.

In [10], we extent our work to propose an empirical path loss model, as well as model verification. This model can be express as:

$$L=\xi r^{\alpha} e^{\beta r} \qquad (8)$$

Where the parameters of path loss factor ξ, path loss exponent α, and attenuation factor β are all functions of the Tx and Rx angles. The parameter a takes a value of 2 for a point source in a free space LOS link, but reduces to 1 in certain NLOS geometries. We then fit the model based on extensive measurements. We observe range dependent power decay with a power exponent that varies from 0.4 to 2.4 with varying geometry. We compare with the single scattering model, and show that the single scattering assumption leads to a model that is not accurate for small apex angles. Our model is then used to study fundamental communication system performance trade-offs among transmitted optical power, range, link geometry, data rate, and bit error rate. Both weak and strong solar background radiation scenarios are considered to bound detection performance.

Using this model, various analytically predicted BER results were demonstrated, and system performance trade-offs were studied in detail, including transmitted optical power, communication range, apex angles, and data rate. These experimental and analytical results are valuable for the design of a practical NLOS UV communication system.

2.4.2 Long Distance Model and Test Results

Because laser can transmit very narrow signal with strong intensity, we take advantage of UV laser for next step experiment to measure IRF and long distance path loss, all of the reported data are collected using the UV laser measurement system depicted in Fig. 2.14.

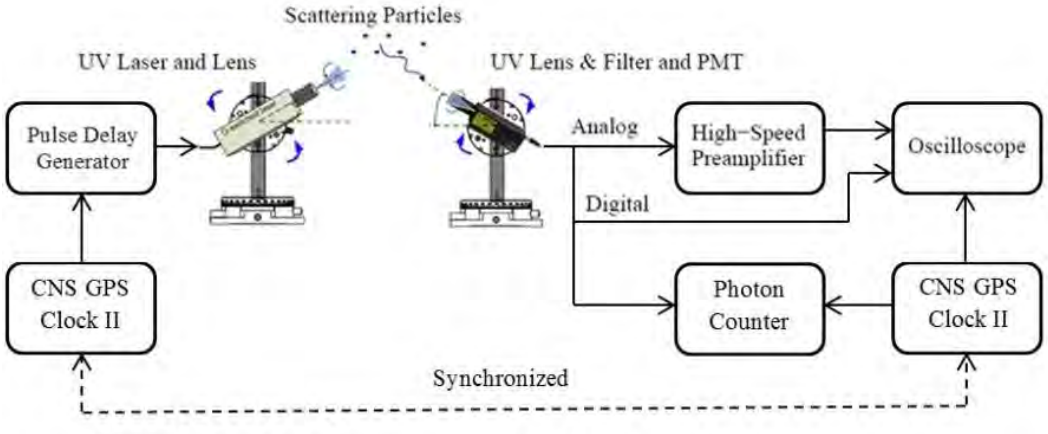

Figure 2.14: Laser based NLOS UV channel measurement system.

In [11] and [12] we present a series of measurements that provide experimental characterization of many aspects of the NLOS UVC channel (including path loss, IRFs, and

pulse spreading) for various system configurations. Pulse width dependence was studied for different system parameters, including Tx and Rx elevation angles, Tx beam angle, Rx FOV, and baseline distance. We found the pulse width was weakly dependent on Tx beam angle variations, but changed almost linearly with other parameters.

Experimental results in [13] that provide reasonable channel modelling validation out to several hundreds of meters also illustrate the measurement error that can result from saturation of the receiver arising from detector dead time. On the other hand, this experiment partially validate the correctness of path loss channel model proposed before. Fig. 2.15 reports sets of these estimates based on the analog and digital systems along with theoretical predictions. The estimates based on the analog PMT agree well with predictions at 758 m, but deviate from both the digital PMT estimates and the theoretical model at 400 m. We believe this discrepancy is in part attributable to measurement distortion arising from the decreasing width of the received signal pulse as range and elevation angles are decreased. Similarly, the digital PMT results agree well with model predictions except at very low elevation angles, where the device has clearly saturated.

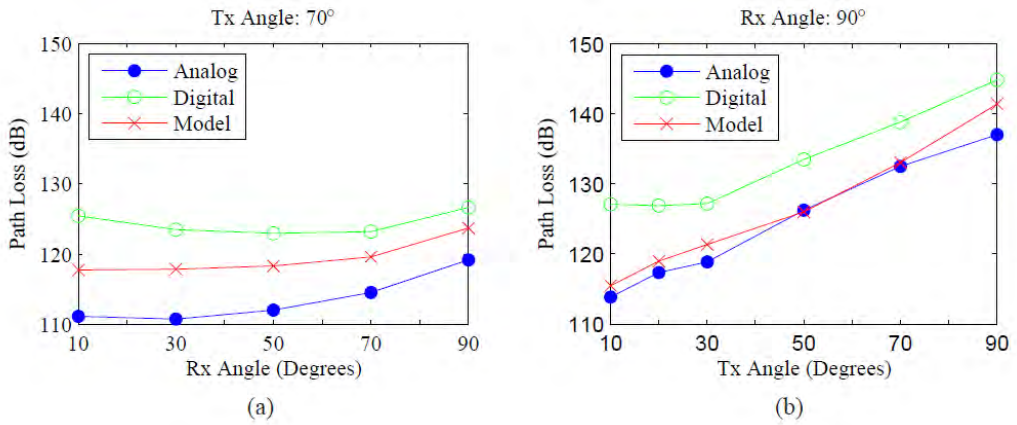

Figure 2.15: Path loss measurements and predictions for a range of (a) 400 m and (b) 758 m.

By putting corresponding attenuator on the top on PMT, we extend our experiment up to several kilometer without the dead time problem [14]. And in this paper, experimental measurements of path loss and pulse broadening effects at distances of up to 4 km are reported and analyzed, and comparisons between the field test data and a Monte Carlo multiple-scattering channel model provide strong evidence for the validity of the theoretical modeling approach.

In addition, measurements probing the effects of turbulence are also considered, but in this case, we find limited experimental support for existing turbulence models, an important result suggesting the need for refined turbulence modeling. Nevertheless, the analytical NLOS UV turbulence channel model proposed in [17] is partially verified. We apply the approximation of the NLOS path as consisting of two segments: the transmitter to common volume and common volume to the receiver. As such, the irradiance at the common volume has a LN PDF

$f_X(x)$, and the conditional arrival power level at the receiver has a LN PDF $f_{Y|X}(y|x)$, where X and Y represent the power levels at the common volume and the receiver, respectively. Lastly, σ_x^2 and σ_y^2 is the turbulence index. The joint PDF for X and Y is therefore

$$f_{X,Y}(x,y)=f_{Y|X}(y|x)f_X(x), \qquad (9)$$

and the PDF of the received power Y is

$$f_Y(y)= \int f_{X,Y}(x,y)dx. \qquad (10)$$

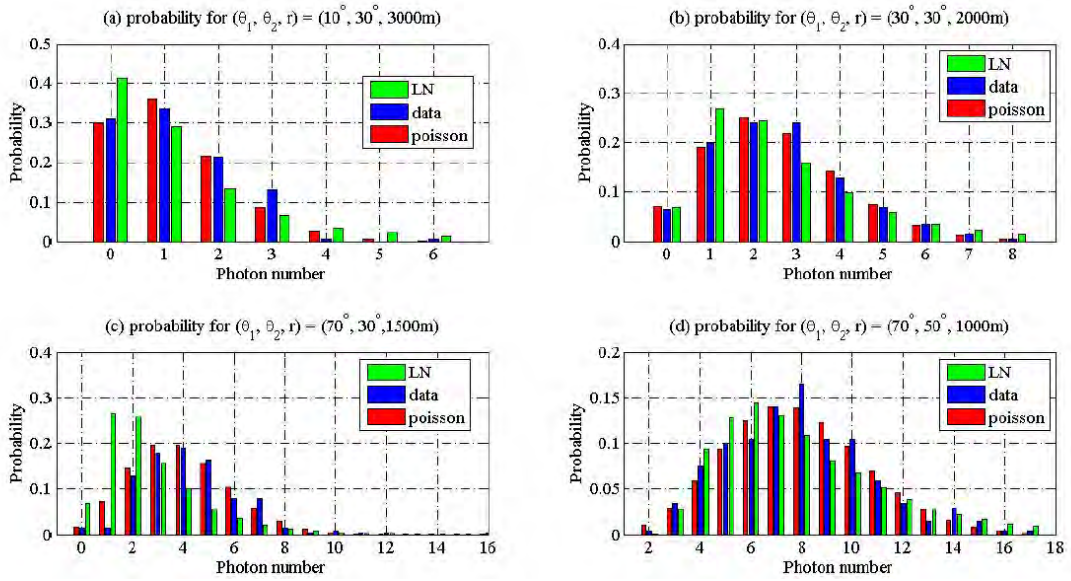

Figure 2.16: Comparison of model predictions and experimental estimates of photon count distributions for four system geometries.

Fig. 2.16 illustrates the estimated received-count PDFs based on the theoretical model and the experimental measurements. We note significant mismatch between the theoretical turbulence-based and measured PDFs, though the general features and characteristics are captured by the model. It is also well known that shot noise contributes to variation in the received counts. Therefore, Poisson PDFs is also plotted as comparison. Clearly, the Poisson PDFs appear to fit the data better than the PDFs based on the turbulence model. As such, it appears that the effects of turbulence (if such effects exist) on the count distributions may be overwhelmed by shot noise. However, with limited sample sizes, the conclusions that can be drawn from this data set may be restricted.

Also, through observing the first hand field test result, we propose that there is extra path loss need to be taken into account, caused by turbulence effect. The scintillation attenuation of each path is given by,

$$\alpha_{r_1} = 2\sqrt{23.17 C_n^2 (2\pi/\lambda)^{7/6} s^{11/6}}, \qquad (11)$$

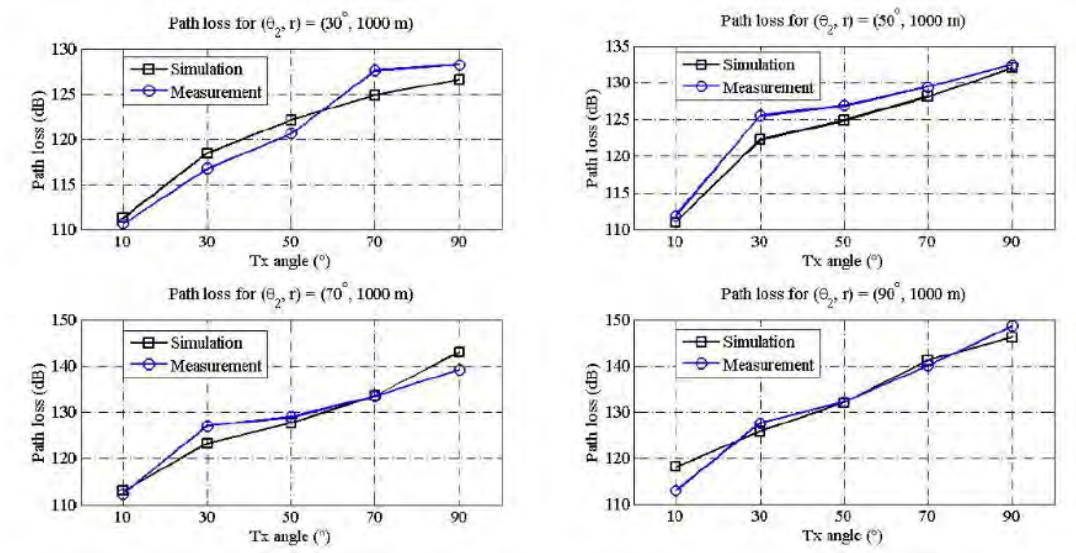

Figure 2.17: Comparison of turbulence-model predictions and experimental estimates of path loss for several system geometries.

Where s is the length of each path. After compensating of the predicted path loss, Fig. 2.17 shows the comparison between path loss estimates with model predictions obtained by applying the theoretical turbulence attenuation to the field test results. Incorporating the turbulence attenuation model has reduced the error between the measured and predicted path losses, supporting the significance of turbulence attenuation in the NLOS UV channel.

3. Advanced UV system with Integrated USRP and GPS

3.1 Motivation

Software defined radio (SDR), where the design flow is mostly in software, makes it useful for fast prototyping of new communication techniques by leveraging the inherent flexibility of software based systems compared to their hardware-based counterparts. To develop a practical UV system and make it compatible with the existing RF communication system, the software defined radio (SDR) based UV multiuser communication system development is necessary for system-level verification and performance demonstration. Upon army's Blue Radio, a USRP based wireless optical communication (WOC) test system is built. The system is designed with the proper interfaces that enable integration with the USRP which was widely used by ARL. This will provide a unique ARL test-bed that includes both optical and radio networking in a single platform, opening the door for significant new research in their combination. The research enabled by this hybrid test bed is built upon collaboration between the PI and ARL scientist.

The second generation programmable radio platform USRP N210 was adapted to incorporate an optical front end. This advanced UV system [18] use state of the art deep UV LED arrays, optical filters, and a very high sensitivity photomultiplier tube receiver. The programmable platform will enable expansion to include optical OOK modulation and built in real time photon counter, as well as integration within a radio network. In some situations of UV NLOS communication, the signal suffers extreme bad communication channel, thus only few photons will arrive at receiver. It's difficult to recovery the clock signal. Therefore, two CNS Clock II are used for generating 10 MHz external reference clock signal and 1pps trigger signal for synchronizing the transmitter's and receiver's USRP platforms.

3.2 Ultraviolet communication system parameter

Due to UV special communication channel, in some particular communication geometries only few photons arrive in one symbol slot, so phase and frequency information are hardly to be recovered in this scenario, while IM/DD (intensity modulated/direct detection) system still works. In this system, OOK modulation and photon counting demodulation are applied. All path loss and BER test results are based on a solar blind GPS synchronized UV communication system at 260 nm wavelength, which is shown in Fig. 3.1. At transmitter side, 2 ball-lens UV LEDs (TO-39) are driven by the amplified modulated signal out of Tx USRP, with 6.5V driving voltage, 60 mA driving current. Each LED gives out 0.3 mW optical power, with 7° beam angle. Through Linux software Gnu Radio, laptop A controls Tx USRP to transmit corresponding signal generated by LFTX (DC-30Mhz) daughter board. GPS servers as the external clock and supplies 10 Mhz reference clock and 1 pps trigger signal. At the receiver side, a commercial digital PMT (Perkin-Elmer photomultiplier tube) with a solar

blind UV filter on top is deployed to convert the received optical signal to electrical signal. The PMT has a built-in current preamplifier and with a circle sensing window with a diameter of 1.5 cm (resulting in an active area of 1.77 cm^2). It has a spectral response from 165 nm to 320 nm, 10 dark counts per second. The peak quantum efficiency of 15% and peak gain of 10^6 occurs at 200 nm, while decreasing quickly towards longer wavelengths, about 10% at 260 nm and 7% at 280 nm. Combining the solar blind filter and PMT, the detector's effective FOV (Field of View) is estimated to be 30° based on measurement. Another GPS at receive side acts as system clock as well. At last, Rx USRP with LFRX (DC-30Mhz) daughter board demodulates incoming signal and then sends to laptop B.

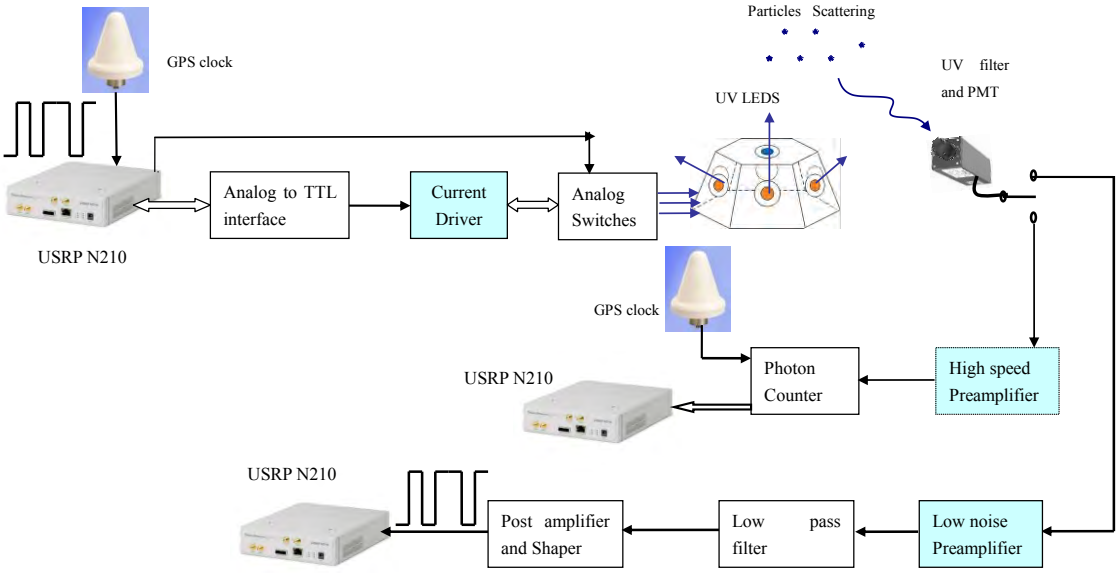

Figure 3.1: NLOS GPS UV USRP communication system diagram.

PMT outputs each pulse with the 20 ns width, corresponding to 50 Mhz. Due to laptop and USRP's limitation, receive side USRP sample rate is only set to 25 Mhz, which means receiver might miss part of photons. Therefore, the communication link cannot be built when the signal strength is too weak. Through GPS synchronization, Rx USRP keeps sampling in time domain to count photons and then makes decision for each symbol base on photon number threshold.

3.3 USRP based UV System Performance compared to model prediction

Three previous proposed path loss models [1][6][10] are used to predict pass loss. We compared practical system BER performance to simulation predicted results with investigating the NLOS UV link path loss, BER and photon count rate, etc.

Table 3.1: Atmosphere model parameter: tenuous, thick, thick plus and extra thick conditions.

atmosphere	$k_s^{Ray}(km^{-1})$	$k_s^{Mie}(km^{-1})$	$k_a(km^{-1})$
tenuous	0.266	0.284	0.972
thick	0.292	1.431	1.531
thick plus	1.101	4.530	1.602
extra thick	1.912	7.648	1.684

Given the power limitation of our experiment LED, we only focus on baseline range from 5 meters to 30 meters. We examine the path loss while varying Tx and Rx apex angles. In our simulation, we assume the same parameters as we discussed in section 2 before. Due to special experimental circumstance, scattering condition were estimate under weather condition from thick to extra thick, whose scattering coefficients can be found in Table 3.1.

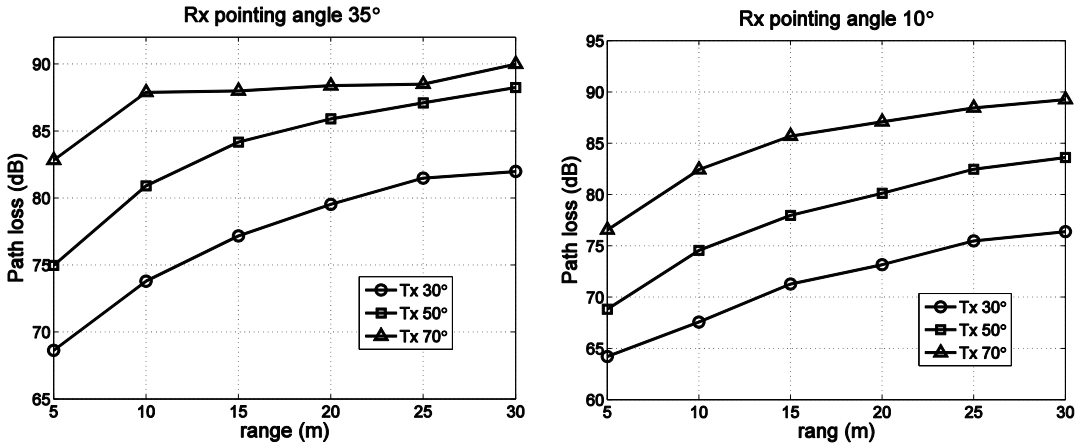

(a) (b)

Figure 3.2: System path loss under different configurations

Fig. 3.2(a) and 3.2(b) depict range-dependent path loss for varying Tx and Rx pointing angles. We can see that path loss is very sensitive to the Tx pointing angles. In particular, for fixing large Rx pointing angle increasing Tx pointing angle may exhibit dramatic path loss deterioration, which implies that it is necessary to increase the transmitted power to compensate the high channel attenuation loss for large apex angle geometry. Due to USRP sample rate's limitation and site's restriction, we only measure path loss up to 90 dB around.

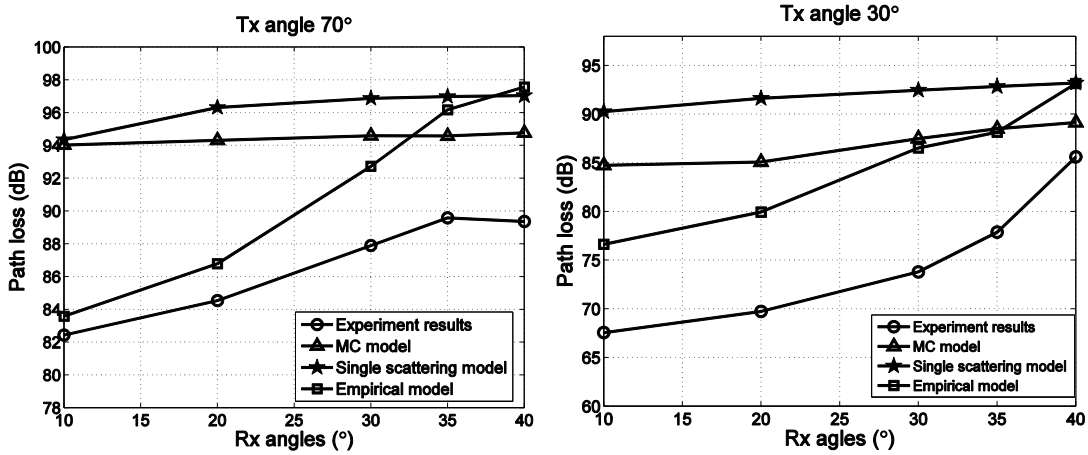

(a) (b)

Figure 3.3 Comparison of measured and simulated path loss results

Fig. 3.3(a) and 3.3(b) compare predicted path loss model with experiment results for Rx angle up to 40° when baseline separation is 10m with Tx angle 70° and 30°. We can see that Empirical model describes path loss tendency well, especially in low pointing Rx angle, but error rises as apex angle increase. Scattering coefficients also intensively impact path loss at short range. Different values of scattering coefficients will lead to 3-5 dB disparity. When both Tx angle and Rx angle are large, MC model's prediction is very close to tested results under thick plus condition, while it deviates from experiment results under low pointing angle. We believe those discrepancies is directly attributable to measurement distortion arising from the partial LOS signal detected by receiver with large FOV as baseline distance and Tx elevation angles are small. This also makes Single scattering path loss model predict inaccurate. What's more, it misses the multiple scattering part, which is relatively high under present weather condition.

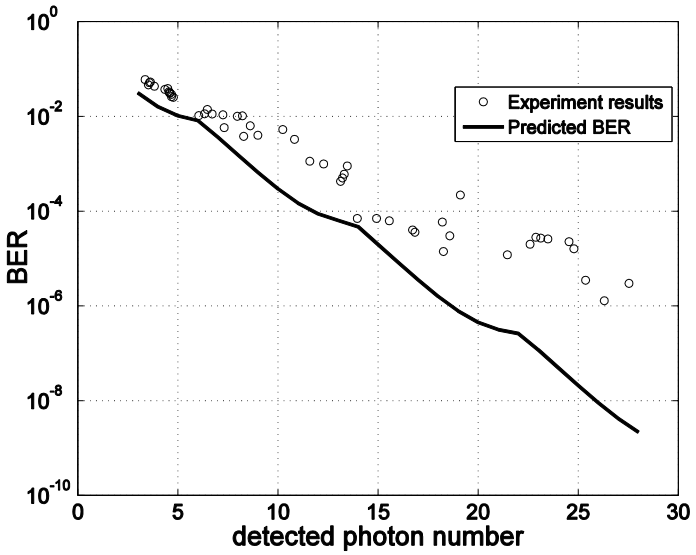

Figure 3.4: Comparison of measured and simulated BER results

As Fig. 3.4 shown, Gaussian noise BER model predicts more accurate than poisson noise BER model as noise count rate low as 140 Hz and signal rate as 10k Hz. Because poisson noise BER model misses other noise sources. When the detected photon number is below 18 per symbol, experiment results fit predicted results very well, but clearly deviate over 20 photons per symbol. The current flow from the filter output, induced by the incident optical wave, is

$$i=i_s+i_N, \qquad i_s=\frac{\eta e P_s}{h\nu}$$

Where, i_N is detector noise and i_s is the signal current. The random shot noise current i_N at the output of the filter is assumed to be a zero mean so the total noise power is defined by [27].

$$\sigma_N^2 = \langle i^2 \rangle - \langle i \rangle^2 = \langle i_N^2 \rangle = \sigma_{sh}^2 + \sigma_{bg}^2 + \sigma_{th}^2 = \frac{2\eta e^2 B P_s}{hv} + \frac{2\eta e^2 B P_{bg}}{hv} + \frac{4k_B T_e B}{R_L},$$

Here P_s is the signal power in watts, η is the detector quantum efficiency in electrons, e is the electric charge in coulombs, h is Planck's constant ($h=6.63*10^{-34}$), and v is optical frequency in hertz. Hence, the detector current noise power is proportional to detected photon number. Thermal noise is caused by the thermal fluctuation of electrons in any receiver circuit of equivalent resistance R_L and temperature T_e. Here, k_B is Boltzmann's constant ($k_B=1.38*10^{-23}$).

This section described our GPS and USRP based advance UV communication system. A set of field test are done outdoor. We compared practical system test performance to three previous proposed path loss models and BER models. All discrepancies are analyzed, which are valuable for short range UV communication system design and proposal for new prediction model.

4. Performance Limits of NLOS UV communication link

- **Fundamental Tradeoffs in a Scattered NLOS UV Link**

The performance of NLOS UV communication through a scattering channel has not been systematically investigated in literature before our work. This research considers the unique features of UV communications such as low noise, high sensitivity and scattering effect and obtains the knowledge on the potential of a short range NLOS UV channel for communications. The study is developed on the assumption of an ideal photon counting receiver. The methodology is to combine into the symbol error equation the path loss model and pulse delay spread which are two most significant characteristics of a scattering channel. Due to the scattering, the optical power has substantial loss before it reaches the receiver aperture; on the other hand, rich scattering creates multiple path of transmission such that the light pulse is expanded. The analysis of link performance has to take into account these two specific aspects.

In what follows, Section 4.1 presents several preliminaries which are necessary bricks to construct our framework of modeling. Section 4.1.2 touches the fundamental question on what is the achievable rate versus range constrained by the given error performance. To improve the limited range of communication due to huge path loss of the NLOS UV channel, we propose the concept of a multi-hop NLOS WoC link to the UV communications in Section 4.1.3. Section 4.1.4 reports the numerical results and findings.

4.1.1 *Preliminaries of UV Communications*

Similarity as an NLOS UV link shares with any WoC system or wireless communication link, the system configuration has its special attributes of flexible geometric link configurations which are illustrated in Fig. 2.1. A NLOS UV communication system adopts the intensity modulation and direct detection (IM/DD), for which the intensity of light is manipulated to represent modulation symbols. Although the background radiation remains a substantially weak level, solar blind filters of 255nm and 271nm can be placed in front of the UV enhanced PMTs such as the Perkin Elmer MP1922 and Hamamatsu R7154 to further reduce unnecessary response to the out-of-band light field. The NLOS UV test bed implemented at the wireless information technology lab (WITLab), University of California, Riverside selects commercial UV LEDs at the wavelength of either 280nm or 250nm as the light source. In the wavelengths of interests, the spectrum on the chosen wavelengths is measured to have a minimum solar irradiance near the ground [22]. The path loss model [1][6][7] characterizes the attenuation of scattering channel on the optical power; another critical feature of the channel is the pulse delay spread due to light signals from multiple paths overlapping and rendering a broadened pulse shape. We measured the pulse broadening in [12], which is summarized in Fig. 4.1.

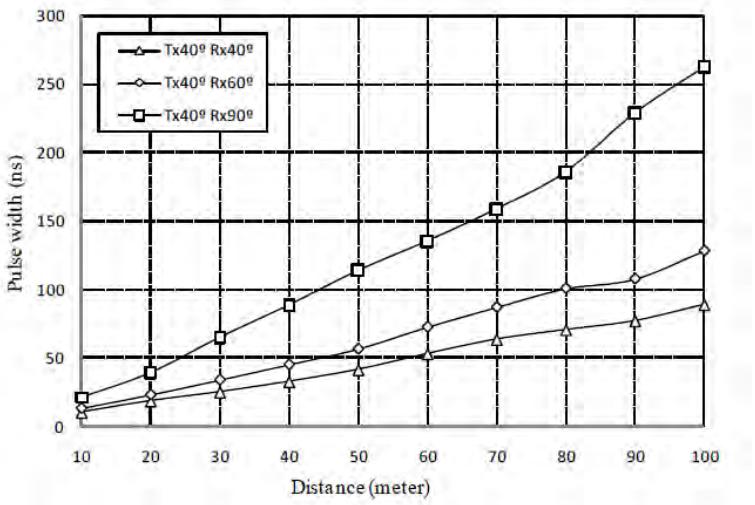

Figure 4.1: Broadened pulse width vs. Tx angles.

The versus Tx pointing angles and propagation distance respectively. With the increasingly severe ISI effect, a NLOS UV system designer must take cautions on the prediction of system capability and seek measures to improve. In our research, the performance projection and analysis is conducted by considering the ISI effect due to broadened pulse.

Inspired by the low background noise and high Rx sensitivity of a NLOS UV link, it is very natural to establish our problem formulation assuming a Poisson photon counting receiver, the output of which is Poisson distributed. Since both OOK and pulse position modulation (PPM) have their modulation symbol represented by the amplitude or position of a baseband pulse (slot), we designate the slot with the signal pulse a signal slot with the time span of T_S. At the photon counting receiver output, the signal photon counts n_s is Poisson distributed with average photon count number of λ_s, which is determined by the instantaneous optical intensity. The average background noise photon count λ_b is mainly contributed by the solar radiation.

The performance of a photon counting receiver to detect the transmitted OOK modulation symbols can be developed by applying the general definition of error probability as in eqn.

$$P_e = \frac{1}{2}\sum_{k=0}^{m_T}\frac{(\lambda_s+\lambda_b)^k e^{-(\lambda_s+\lambda_b)}}{k!} + \frac{1}{2}\sum_{k=m_T}^{\infty}\frac{(\lambda_b)^k e^{-(\lambda_b)}}{k!}.$$

So we have the error probability is derived by considering a threshold based detection. The decision unit at the receiver recovers the modulated binary data by comparing the photon counts for each OOK symbol with the pre-defined threshold m_T. If we minimize *Pe* with respect to m_T, an optimal threshold is given by

$$m_t = \left\lfloor \frac{\lambda_s}{ln(1+\frac{\lambda_s}{\lambda_b})} \right\rfloor.$$

We also consider the use of optical block encoding [28] achieved by converting every block of *b* bits into one pulse out of every $M = 2b$ orthogonal slots. One popular form of such block coding is pulse position modulation (PPM). One of the reasons PPM is favored by communication designer is, first of all, the simple decision rule. The receiver does not need to compute and maintain a threshold, instead compares the photon counts across all slots and chooses the slot with the most counts as a maximum likelihood method in nature. Secondly, PPM is advantageous to recover the symbol clock even when there is a long sequence of zeros. We leave the performance study of PPM modulation in the context of a Poisson counting receiver in the ensuing sections.

To conclude, the understanding of communications through the scattering channel relies on the correct characterization of the path loss and pulse delay spread. The prediction on achievable performance assumes pulse based modulation and photon counting receiver.

4.1.2 Range versus Rate for Short Range NLOS UV Link

We are motivated to study the topic of range versus rate because the scattering effect dominates the transmission and the path loss for NLOS UV is enormously larger than that of line-of-sight (LOS) link. The two modulation schemes are OOK and PPM and we start with the general case where the background noise is nonzero. Then we derive simple and closed form results for shot noise limited case, which eases the derivation of more intuitional results. Range-Rate Performance of OOK. A numerical approach of computing the tradeoff of range *r* versus rate *Rb* can be summarized as below.

- *Achievable Performance with PPM*

When PPM is adopted as the modulation scheme, the decoder needs to determine which slot of the PPM symbol contains the pulse before demapping it into encoded bits. A decoding error happens when incorrect slot has higher integral value than the correct slot. The symbol error probability of an M-PPM system is given in [28] and according to the relationship between symbol error rate and bit error rate [29], the resulting bit error probability is

$$
\begin{aligned}
P_e =& \frac{M}{2(M-1)}\left\{1-\int_0^{\infty} p(\nu_1|1)\left[\int_0^{\nu_1} p(\nu_2|0)\nu_2\right]^{M-1} d\nu_1\right\}, \\
=& \frac{M}{2(M-1)}\left\{1-\frac{e^{-\lambda_s+M\lambda_b}}{M}-\sum_{r=0}^{M-1}\frac{(M-1)!}{r!(M-1-r)!(r+1)}\times\right. \\
& \left.\sum_{k=1}^{\infty}\frac{(\lambda_s+\lambda_b)^k e^{-(\lambda_s+\lambda_b)}}{k!}\left[\frac{\lambda_b^k e^{-\lambda_b}}{k!}\right]^r\left[\sum_{j=0}^{k-1}\frac{\lambda_b^j e^{-\lambda_b}}{j!}\right]^{M-1-r}\right\},
\end{aligned}
$$

p(v1 |1) is the probability density function when correct slot has a pulse and p(v2|0) is the probability density function specifying the rest slots indeed have an integral less than the counts in the correct slot.Note that the relationship between *r* and *Rb* for PPM modulation can be readily evaluated numerically.

4.1.3 Extending the Range of NLOS UV using Multi-hop Technique

Previous discussion has indicated the UV communications leverages the benefits of an NLOS path and covertness of limited range, both ensured by the scattering channel. Nevertheless, by flipping the coin, there are down-sides such as the huge path loss, which impose unique and harsh requirements on the system design to achieve desired performances in range and data rate. For instance, increasing the power is a common and straight forward method to improve communication performance, but a wireless optical communication (WOC) system must consider the regulations on human eye safety. Also, the convenience of deployment favors light-weight and compact transceivers. The performance of NLOS UV link for communications based on point- to-point transmission has been addressed in section 4.1.2. In this section, we propose a multihop system configuration to reduce the transmitter power consumption and the number of LEDs while extending the communication range.

Relayed mesh network in radio frquency domain has a rich history and is comprehensively reviewed. Regarding relayed FSO links, note that there has been some work in recent years, [30][31][32] , but most of them assume line-of-sight (LOS) conditions and focus on outage analysis in a fading environment because of turbulence effects. By contrast, we study the performance of NLOS UV multihop network by incorporating the path loss model specific to NLOS UV channels and neglect the effect of turbulence by restricting the range of each communication link within hundreds of meters. In light of the low noise characteristics of a solar-blind UV system, the performance analysis follows a classical model, i.e., intensity modulation with direct detection (IM/DD). The transmit power with on-off keying (OOK) modulation is obtained for the case of direct transmission as an example illustrating why the NLOS link is power starved. We next obtain the power for individual relay node in a serial multihop configuration using a decode-and-forward scheme aiming to prove the benefit of power saving. We show how the interference in a NLOS multihop system results from the nature of directional transmission and reception, and the performance degradation is evaluated versus link geometry and the number of hops. Accordingly, a spatial reuse technique of coordinated transmission and cooperative reception is suggested in section 4.1.4.

- *A Multi-hop NLOS UV Link*

Let us examine a multihop topology for a NLOS UV communication link aided by relay nodes in Fig. 4.2. The source transmits an OOK modulated signal to the first relay node through a NLOS channel. Each relay decodes and forwards the received symbols to the next relay and so on. From the source to the destination, there are $N+1$ nodes equally dividing the range of communication into N segments. We specify the same system geometry for both direct transmission and the relaying segments.

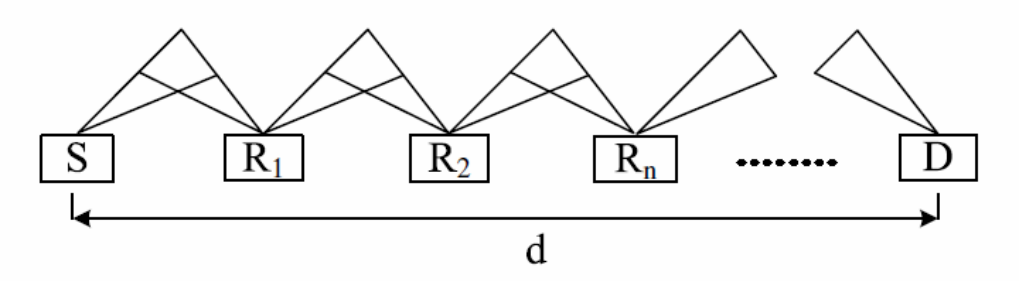

Figure 4.2: A NLOS multi-hop UV communication link.

To evaluate the transmit power for each node in the serial multihop link, we study the end-to-end error performance P_{eMH} and throughput R_{bMH}, equal to *Pe* and *Rb,* for direct transmission. With decode and forward (DF) operation at each relay, it is natural to obtain the end-to-end error performance as:

$$P_{e_{MH}} = 1 - \prod_{n=1}^{N}(1 - P_{en}) = 1 - (1 - P_e)^N,$$

Where P_{en} is the piecewise error probability for the nth hop

Besides the question of how the transmit power can be reduced with the number of relays, the other issue with the NLOS multihop UV link is that each relay node sees interference from the previous relays when simultaneous transmissions are allowed to enhance the throughput. Because of the NLOS directional nature, a serial relayed NLOS UV link differs from other existing FSO communication link such as [31]. The LEDs illuminate over a NLOS geometry and the emitted optical field can also be detected by the downstream relays in addition to the immediate destination due to the scattering effect. In other words, an intermediate relay node could see the ”blinking” light from more than one upstream relays. The situation is shown in Fig. 4.3.

For non-coherent detection of the intensity, the interference raises the noise level, and the quantum limited assumption no longer holds. We employ a general treatment in the error analysis of OOK modulation to examine the performance with interference.

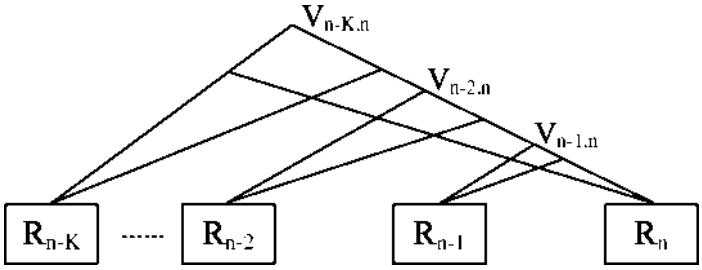

Figure 4.3: A multi-hop NLOS UV communication link with directional interference.

In Fig. 4.3, the n_{th} node can receive the signal of interest from the $(n\text{-}1)_{th}$ node and interference signals from the $(n\text{-}2)_{th}$ up to $(n\text{-}K)_{th}$ nodes assuming simultaneous transmission is permitted with no coordination. *K* is defined as the number of upstream interfering nodes for the $(n\text{-}1)_{th}$ node. The interfering nodes are termed upstream nodes leading the $(n\text{-}2)_{th}$ node. The piecewise error probability for the nth hop is conditioned on the on-off symbols transmitted by the interfering nodes, given by

$$P_{en_{intrf}} = \frac{\sum Pr\{\hat{x}_n \neq x_{n-1} | R_{n-2}, R_{n-3}, \ldots, R_{n-K}\}}{2^{K-1}}.$$

The calculation has to average over all the possible interference patterns. An upper bound is the case when ”1” is transmitted from all upstream nodes. For example, consider K = 2 where only one interfering node sends ”1”. The intensity of the interference signal depends on the path loss. Since $L_{n\_2,n}/L_{n\_i,n} = 2^a$, the number of interference photons during each symbol interval becomes $\lambda_i = 2^{-a}\lambda_s$, which may significantly raise the noise level.

The directional interference problem arises because the relay nodes are permitted to transmit at the same time. If we arrange the transmission of each relay node in a non-overlapping time slot, it is obvious the interference is avoided at a cost of N times longer in the end-to-end delay. In this regard, we adopt spatial reuse through orthogonal time sharing that helps to minimize the directional interference and improve the throughput by a reasonable assumption that photons die out beyond a certain range and create no interference. Since we may virtually put *K* interfering nodes into one group and the node after every *K* relays may reuse the channel in terms of either time slot or frequency, *K* is also regarded as the spatial reuse factor. To design an effective transmission protocol, the *K, N* and hop length are major knobs to design. We’ll assess the effects of these parameters on piecewise error performance through numerical methods.

Even though spatial reuse is employed, one has to be aware that interference may still result from the node which precedes the reuse group and transmits in the same slot position. This may deteriorate the spatial reuse performance to some extent and we thus propose a cooperative reception scheme built upon spatial reuse to fully harvest the photons from the transmissions of the nodes in the same spatial reuse group.

The mechanism is explained in Fig. 4.4. If we set the spatial reuse size to be K = 2, R2 and R3 belong to a spatial reuse group, each reserving one time slot for transmission to their next relay. Hence R4 is immune from the interference due to R2's transmission when R3 relays to R4 in slots T3; T5; T7 ⋯. Because the spatial reuse is arranged every K relays, the nodes S, R3; ⋯; R_{2n+1} share the same slot in time while R2; ⁃ ; R_{2n} reuse a different slot. Thus the interference will only be contributed from the relay node in the previous reuse group that transmits in the same time position, namely, node S. Further, consider the cooperative reception in slot T3. Node R4 com- bines the signal from R3 and the copy previously received in T2 from R2. Since in an optical transceiver, the Rx and Tx are separate branches which provide the full duplex capability, R4 is capable of both relaying and receiving in T2. This consists in the basis for the cooperative reception.

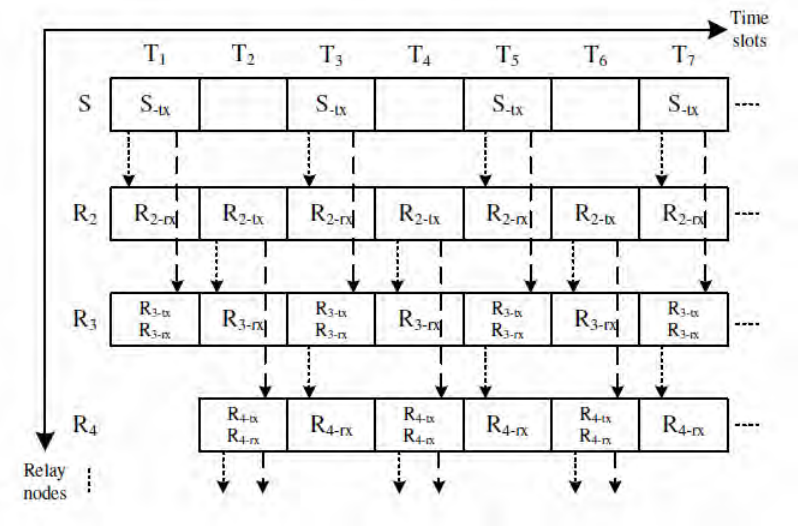

Figure 4.4: Transmission and receiving protocol for multi-hop NLOS UV link, $K = 2$.

4.1.4 Numerical Results for NLOS UV link

This section reports the numerical studies on NLOS UV link through the scattering channel. We start with the point to point scenario and then extend the discussion to a multi-hop configuration. These results provide useful reference for system design. Following numerical results are depicted in Figs 4.5-4.10, which are cited from our published papers [33][34][37]:

- *Range and Rate of Point-to-Point NLOS UV Link*

We further incorporate an empirical path loss model for an NLOS UV link into bit error probability analysis for a photon counting receiver to characterize the achievable performance in terms of the baseline range and bit rate. It can be shown that the performance largely depends on the system geometry defined by pointing angles.

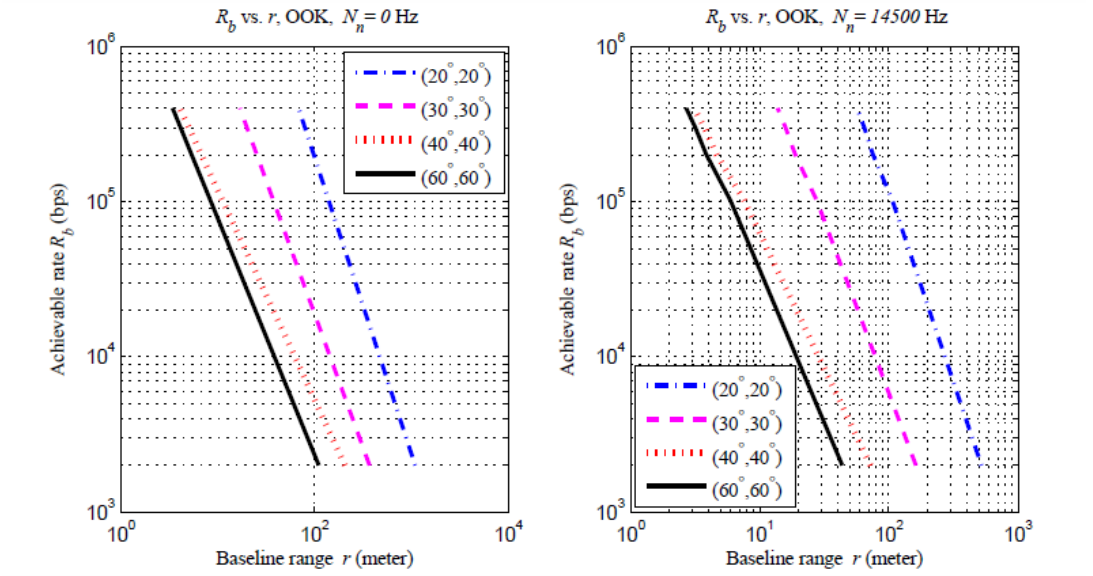

Figure 4.5: Achievable rates vs. base-line range for OOK modulation, P_t =50mW; $P_e = 10^{-3}$, low noise (left) and high noise (right) cases.

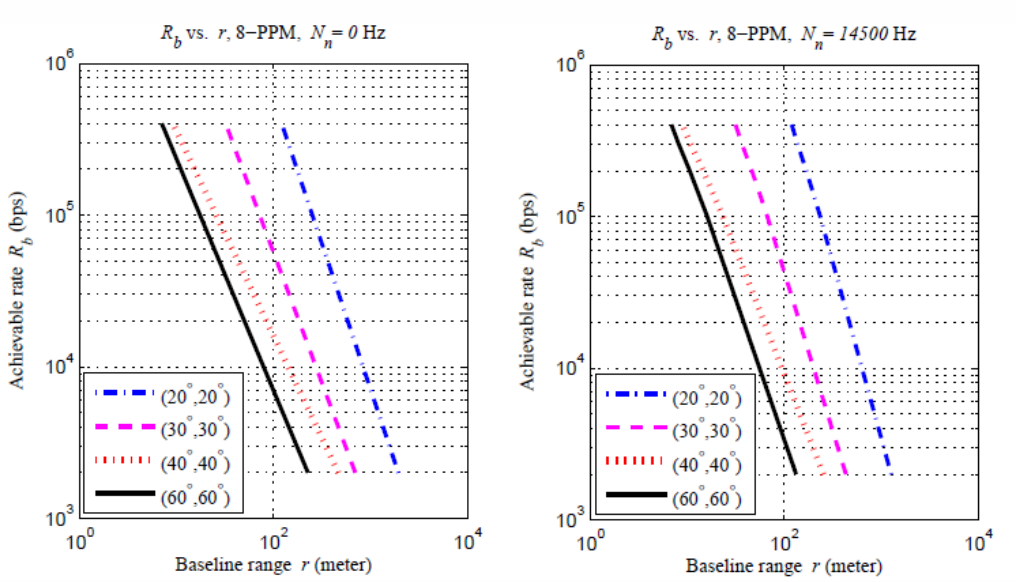

Figure 4.6: Achievable rates vs. base-line range for 8-PPM modulation, P_t =50mW; $P_e = 10^{-3}$, low noise (left) and high noise (right) cases.

In Fig. 4.5, both shot noise limited case and regular background noise case are plotted. Over the range of 100m, with the requirement of 10^{-3} in error probability, a rate of 1k-100kbps can be expected from high elevation angles to low elevation angles given 50mW of transmission power. When there is certain background noise due to solar radiation, achievable rate has some loss on the order of 10% less than that of shot noise limited case. By comparing Fig. 4.5 with Fig. 4.6, more than 30% increase in data rate can be boosted with higher order PPM modulation scheme. It is worthwhile to note that since we focus on uuencoded error performance, according to Shannon capacity in the perspective of information theory, extremes of range and rate shall be much higher than what we illustrate. Recently, ways to achieve the Shannon limit have been extensively and intensively studied by the coding community via graph based error control codes like LDPC codes and iterative decoding. Even without those probabilistic codes, conventional algebraic codes can be applied to improve the performance. For instance, [39] gives a Reed Solomon code based method. Interested readers are advised to read the references and therein. Our research is mainly oriented in the analysis of raw bit error rate and less touches the scope of error coding and decoding techniques.

- *Multi-hop NLOS UV Link Performance*

In this section, we intend to prove the benefits of a serial multi-hop link configuration for NLOS UV communications which can save not only the power of individual relay node but also the overall power consumption of the whole link. Notice that the interference effect due to the neighboring nodes will cause higher piecewise error probability, we study the effect quantitatively. The key system parameters are summarized in Table 4.1.

For a quantum limited case, the predicted power is shown in Fig. 4.7 that Tx/Rx pointing angle pairs (10°, 10°)，(20°，20°)，(30°，30°) and (40°，40°) call for emission power 15mW, 150mW, *1W*, and 2.5W over the range of 300meters respectively. Although the power on the order of tens of milliwatts can possibly be supplied by a LED array made of a large

number of LED cores at the transmitter, the power on the order of watts at current state of the art can only be provided by a UV laser, which is prohibiting in cost and cumbersome.

Table 4.1 Typical parameters for UV NLOS link

Parameter	Value
Tx apex angle θ_1	$10°, 20°, 30°, 40°$
Rx apex angle θ_2	$10°, 20°, 30°, 40°$
Wavelength λ	250nm
Single LED power P_t	3mW
Information rate R_b	64kbps
Noise photon count rate N_n	$14500s^{-1}$
PMT efficiency η_{PMT}	30%
Optical filter efficiency η_{filter}	20%

By adopting the configuration of a multi-hop NLOS link, the power requirement on individual relay nodes can be relaxed by increasing the hop number. Equivalently speaking, total power is distributed to to spaced relay nodes, each of which consumes much less power. To conclude, adding more relay nodes with a fixed transmission power is an effective way to extend the range of communications. We plot in Fig. 4.8 the node power versus hop number for a multi-hop link at a range of 300meters. For small angle geometry like (10°，10°）and (20°，20°), the transmitter of each node only needs one or seven LEDs to provide $10mW$ power since the effective emission power per UV LED at 250nm is around 1mW. For large angle scenarios such as (30°，30°) and (40°，40°), 30mW and $150mW$ are desired for a 10-hop link over 300 meters. Such a power consumption renders possible the LED array as the light source, which is compact and lightweight. On the other hand, it is clear the overall power consumption could be saved as reflected by the power saving ratio. We plot it in Fig. 4.8 and find out more than 60% of power can be saved when $N > 5$ for all angles except (40°，40°）and the path loss exponent a is a determining factor. In word, it is always beneficial to get decreased individual power consumption through the use of more hops.

For the cons, we are able to identify that simultaneous transmissions of relay nodes cause interference, which largely etches the link performance. The issue can be illustrated in the link error probability in Fig. 4.9. By assuming each hop is adversely affected by the transmission of its nearest upstream hop. For a 10-hop link, without coordination of transmission, performance is demonstrated in Fig. 4.10. Interference has lowered the performance by four orders of magnitude from 10^{-6} to 10^{-2}.

This constitutes the motivation to considering a spatial reuse scheme with cooperative reception. In essence, the idea is that the separation of simultaneous neighboring transmissions shall be enlarged while cooperative reception collects more signal energy from the relay nodes in the same spatial reuse group.

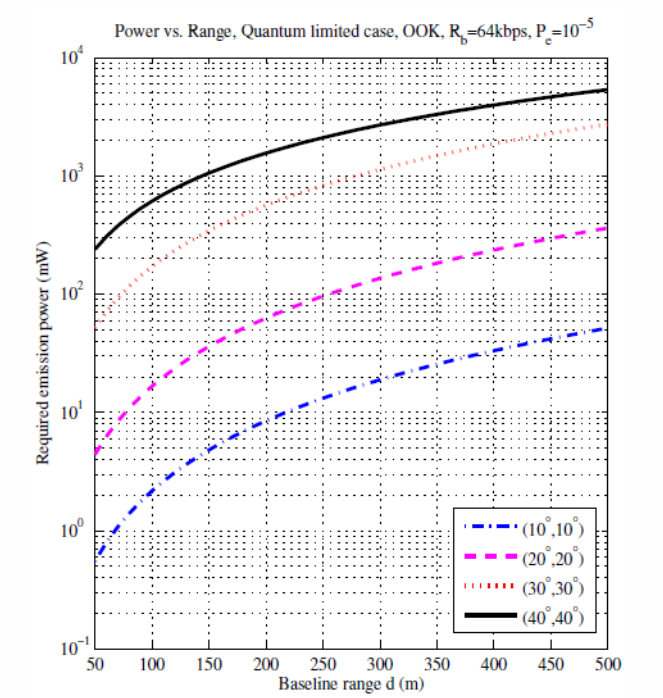

Figure 4.7: Required emission power vs. direct transmission range, quantum limited case, OOK modulation, R_b = 64kbps, P_e =10^{-5}.

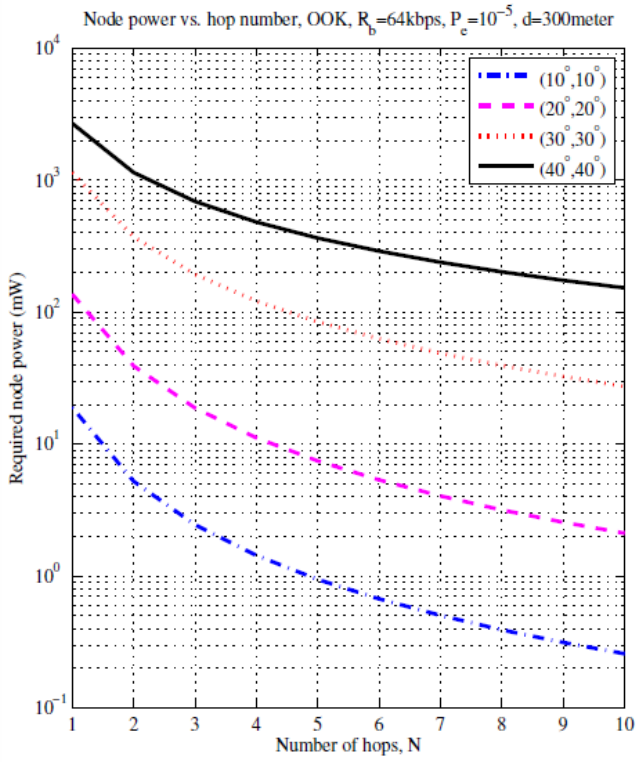

Figure 4.8: Required emission power per relay node vs. number of hops over 300 meters, quantum limited case, OOK modulation, R_b = 64kbps, P_e =10^{-5}.

- **Summary**

In this research, we incorporated an empirical path loss model for an NLOS UV scattered link into the bit error probability analysis by assuming an ideal model of a photon counting receiver. Since the UV channel is strongly affected by the scattering, the path loss model we

considered captures such effect. Numerical methods are employed to illustrate the performance in terms of the tradeoffs of range versus rate. It is shown that the performance largely depends on the system geometry defined by pointing angles. These results provide useful reference for system design.

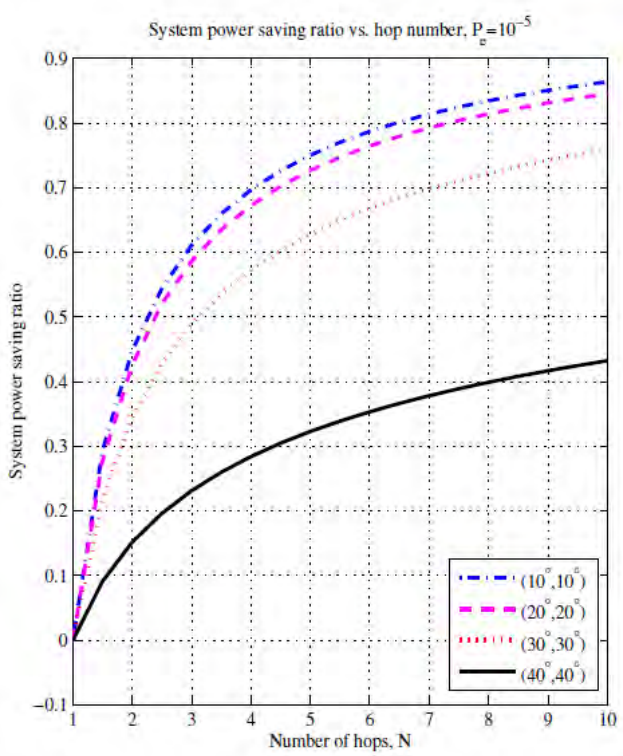

Figure 4.9: System power saving ratio with multi-hop link, $P_e=10^{-5}$.

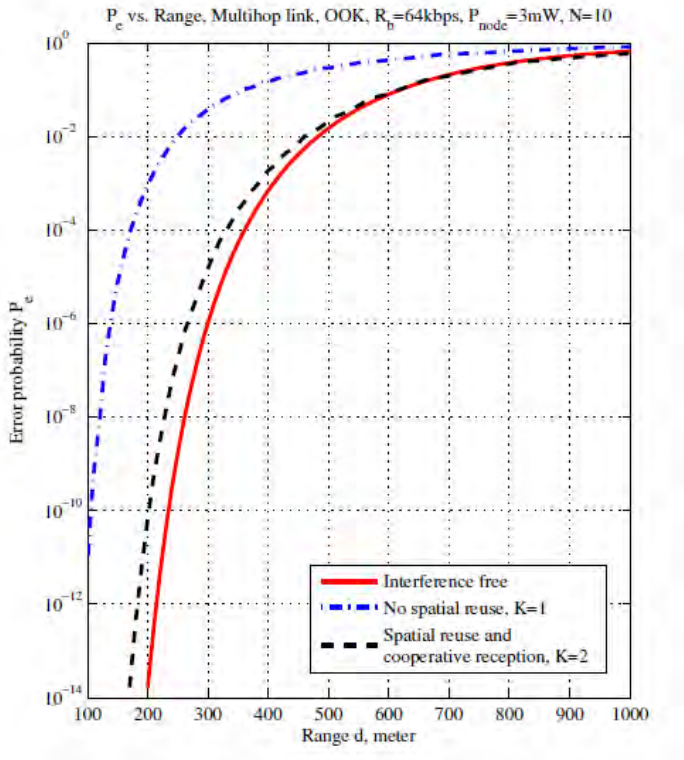

Figure 4.10: Error performance vs. range for multi-hop link, (20°; 20°), node power P_t = 3mW; N = 10.

To improve the link performance and envision a feasible solution for the transmitter of NLOS UV communications, we also evaluate the power saving advantages of a multi-hop configuration, compared against the direct transmission. To alleviate the interference issue, we propose a cooperative reception scheme enabled by coordinated transmissions within each spatial reuse group. We show that the multi-hop scenario can relax the power requirement of both individual nodes and the entire system, which makes NLOS UV a viable solution for wireless sensor network

5. MAC design for multi-user UV network

This chapter mainly focuses on the higher layer protocol design for UV communication networks: medium access control (MAC) protocol design and neighbor discovery methods for deep UV outdoor communications (UVOC). For UVOC, solar blind and NLOS operations are attractive. Light beams from UV light-emitting diode (LED) arrays propagate through scattering media, creating spatially different communication links. This unique physical (PHY) layer characteristic was first captured experimentally based on a UV test-bed, from which mathematical signal propagation models were developed and their impact on MAC design was realized, i.e., full duplexing and multi-rate transmission. It can be observed that none of the existing protocols addresses non-line-of-sight scattering based optical transmission and reception. In this work, we designed a suitable MAC protocols and neighbor discovery methods for free space communications in the UV band.

First we propose a novel contention-based MAC protocol (UVOC-MAC) that inherently accounts for the UV PHY layer and fully exploits multi-fold spatial reuse opportunities. Evaluations via simulation and analysis show that UVOC-MAC effectively mitigates collisions and achieves high throughput. We further develop efficient neighbor discovery protocols by accounting for the varying channel qualities along different scattering directions. Besides a list of neighbor nodes' identities, a ranked list of node pointing directions in terms of channel qualities was also included in the constructed table to facilitate the process. Utilizing neighbor feedback or alternating a leader node were proved to be able to alleviate the negative effects of random access based collisions and thus expedite neighbor discovery.

5.1 UVOC MAC design

- **Motivations for MAC design**

Through the literature review, we note that there has been limited work done on higher layer protocol design for optical wireless communications, particularly in outdoor UV communication (in which we consider ad hoc topology) and indoor VLC (in which we prefer infrastructure topology).

Path loss model for UV communication: For UV communication, there are some prior work on channel modeling including both analytical path loss model [1] and experimental model [10]. Those models capture coplanar NLOS scattering path loss under the motivation of Reilly's common-volume single scattering theory [15]. In a network setting, there is no guarantee of co-planarity of the beam axis and the FOV axis. The coplanar path loss models [1] [10] presented in require the transmission beam axis and the receiver FOV axis to lie in the same plane. The more recently proposed non-coplanar numerical path loss model in [4] and analytical approximate model in [5] capture the effect of partial alignment.

MAC design for UV outdoor communication: The IEEE 802.11 standard proposes a carrier sense based MAC scheme for indoor IR with LOS communication links. The MAC design in wireless infrared communications suggests the usage of CSMA/CA in indoor IR ad hoc networks. There is very limited work in the literature on outdoor OWC MAC. The infrastructure-based MACs are not suitable for ad hoc outdoor scenarios or battlefields. Most importantly, the existing approaches are based on carrier sensing; given the modulation strategies and channel asymmetry those are not appropriate for UVOC. To elaborate, it is unclear whether it is appropriate to assume possible full-duplex communications on both directions of

a UV link. Since PPM is used, carrier sensing cannot be used to infer whether or not transmissions are ongoing. Finally, transmissions at lower rates may interfere with transmissions at higher rates but not vice versa.

Given the narrow beam angle of wireless optics, the communications are directional. There exist many MAC protocols for use with directional antennas in RF [40]--[47]. The natural question that arises is whether these protocols can be directly applied in our considered context (although they are designed for RF). Due to the nature of UVOC, they are not directly applicable. First, physical carrier sensing is not possible with UVOC. Second, they consider spatial reuse only in directions; here, we consider additional dimensions (pointing angle and data rate). DMAC [40] uses directional RTS/CTS to increase communication range, but suffers from deafness. Tone-DMAC [41] uses out-of-band signaling to solve the deafness problem. Out of band signaling requires the use of a different wavelength in OWC. In optics, switching across different wavelengths requires expensive filters and low-speed mechanical operation; further, it is difficult to implement multiple filters in a small portable device. Protocols such as [42] also use carrier sensing. CRM, CRCM, MDA and DMAC/DA [43]--[47] use circular RTS/CTS to avoid the coverage asymmetry problem. A circular RTS/CTS is unnecessary in the context considered. A transmitter can simply turn on all LEDs as shown in all directions at the same time in Fig. 5.1 without causing the asymmetry problem.

5.1.1 Design of the UVOC transceiver

Our system design is shown in Fig. 5.15.1. The rationale behind our design is as follows.

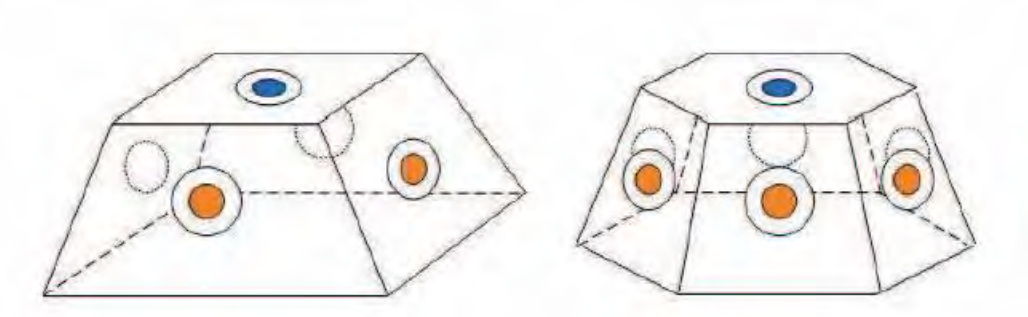

Figure 5.1: System design of the UVOC transceiver with 4 (left) and 6 (right) transmission directions (Dots on the side facets are the directional LED transmitters; dots on the top facet is the omni-directional photon receiver).

Since the photon detector is of high cost but the LEDs are of low cost, it is economical to implement multiple transmitters and a single receiver on a node. Given the dependencies between the pointing angle and full-duplex communications, a good design will be for a node to have multiple surrounding transmitters and a receiver on top. This configuration provides favors to easy installation and deployment on the helmet of a soldier or on the top of a vehicle. In Fig. 5.1, the dots on the side facets represent the LED transmitters (a transmitter could consist of multiple simultaneously emitting LEDs) and the dot on

the top facet represents the omni-directional photon detecting receiver. With this configuration, the node1 is a “directional transmitting" and an “omni-directional receiving" device.

Note that the real implementation is not limited to the shape or the number of facets. The number of directions or facets is determined by the transmitting beam angle. For example, if the beam angle of an LED array on a side facet is 18°, then this device can have up to 20 side facets. In other words, the number of directions is a tunable system parameter.

5.1.2 UVOC MAC description

UVOC-MAC is a random access slot-based protocol. A single UV pulse is transmitted in each slot. The size of a generic slot is a multiple of what we call the unit slot size; the unit slot size corresponds to the highest data rate. The key feature of UVOC-MAC is that it exploits spatial reuse by adaptively choosing: (1) the direction, (2) the pointing angle and, (3) the data rate. Recall that the data rate is determined only by the delay spread which is different for different pointing angles.

- *UVOC-MAC overview*

In the default case, nodes are in the idle state where they simply decode received control signals. Once there is new data from the upper layers (network), a node first checks certain tables to see if the desired communication is possible at that moment and if so, to decide on the best configuration for use. It then chooses a full-duplex mode or a half-duplex mode depending upon whether or not the selected pointing angle is less than or equal to 40°. Based on our experiments data, we assume that with pointing angles less than or equal to 40°, full-duplex communications are possible; if the pointing angle is higher, then only half-duplex communications are possible.

The source and its destination exchange request-to-send (RTS) and clear-to-send (CTS) messages at a base rate R_t (we use similar nomenclature as in 802.11 for ease of presentation; however, the RTS and CTS messages are different here). The RTS message indicates the selected pointing angle; this also implicitly conveys the selected data rate (as discussed earlier, different data rates are possible with different pointing angles). Upon receiving the RTS, the receiver performs certain checks and replies with a CTS indicating the highest possible data rate (based on its interference patterns). The CTS is omni-directional by default and allows neighbors to update their neighborhood information. Then DATA is however sent directionally. There is a data rate announcement (DA) portion at the beginning of DATA frame. It is sent at the base rate and used to confirm the rate at which the remainder of the DATA is sent.

- *UVOC-MAC in detail*

Next, we describe the UVOC-MAC in greater detail. We first describe a few data structures that are maintained for various purposes.

Connection table: Each node maintains a separate Connection table per neighbor. The table specifies the possible directions and pointing angles the node can use to communicate with this neighbor. The entries (an entry defines a combination of a direction and pointing angle) in the table are ranked in ascending order. There is more than one way to rank the directions and pointing angles. We compare two

methods that can be used to rank entries in the Connection table. The space complexity of Connection tables is O{(# of neighbors)·(# of directions)·(# of pointing angles)}.

Occupancy table: This table is maintained at each node and is updated when the node realizes that a new transmission is going to take place in its neighborhood. To elaborate, when a CTS is received from a neighbor node y, a node first checks the Connection table associated with y. It then sets timers in the Occupancy table corresponding to those entries which define transmission configurations that would interfere with y's reception. The space complexity of this table is O{(# of directions)·(# of pointing angles)}.

Rate table: This table stores a record of the data rates in use in the owner's neighborhood. As we discuss later, this information is used by the node to appropriately choose a transmission rate (pulse width) when it acts as a transmitter. The table is updated when the owner checks the first part of every directional DATA packet that it overhears; we refer to this part of the data packet as the "DA" (data rate announcement). The space complexity of this table is O{# of pointing angles}.

Receiving nodes table: This table enlists those neighbor nodes that are currently receivers and the time up to which they remain in the receiving mode. The contents of this table are disseminated using signaling messages and are used to combat effects such as deafness (explained later). The space complexity of this table is O{# of neighbor nodes}.

Next, we look at specific functions that a node invokes with UVOC-MAC.

Check table: A procedure check table is invoked in two cases: (a) when there is new data to send and (b) when a CTS is to be sent. In the first case, the source node checks the Connection table and Occupancy table to find the best combination of direction and pointing angle for use. If the best configuration (with the highest rank) is not available, it has to select an available configuration with a lower rank (it checks each possibility in descending order of rank). If a CTS message is to be sent in response to an RTS, the node checks the Occupancy table and transmits the CTS in all available directions with the lowest available pointing angle. The available directions are defined as those directions that are interference-free; this means sending from these directions will not cause interference to other ongoing communications.

Frame control	Source and direction ID	Destination ID	Duration	Selected Angle	Frame body	Time to wait	FCS	Gossip signaling

Figure 5.2: MAC frame format

Update tables: Every node has to update its aforementioned tables. The tables are updated with different stimuli and periods. The Connection table is constructed during the neighbor discovery process and updated by a neighbor maintenance procedure. Most neighbor discovery and neighbor maintenance schemes applied in networks with directional antennas can also be applied with minor changes in UVOC networks; thus, we can simply leverage these approaches. The implementation of specific neighbor discovery mechanisms for UV is out of scope of this thesis. In this section, we assume that the neighbors of a node are known for simplicity. We explore this in more detail in an associated next section. The Occupancy table and Receiving nodes table are updated upon receiving appropriate control signals and

DATA packets. A node examines the source ID in a CTS message. It also check the IDs of other receiving nodes from what we call the gossip portion (discussed later) in both the RTS and CTS messages. Finally, it checks the duration fields in the CTS, RTS and DATA messages. The Rate table is updated upon decoding the DA portion of every overheard DATA packet.

Gossip signaling: In order to mitigate the hidden node and deafness problems, nodes include information on receiving nodes in their neighborhoods, in the RTS and CTS messages. Note that only partial information can be sent with each message; only a subset of the nodes in the Receiving nodes table can be specified. There is a trade-off between the overhead incurred from the information (amount of information) and the efficacy in combating the aforementioned problems.

- *Frame structure*

The frame structure with UVOC-MAC is shown in Fig. 5.2. The Duration field specifies the time duration of the communication. The Selected angle field specifies the pointing angle suggested by the receiver. The Time to wait field is used in relation to full-duplex communications. For instance, if node A is sending RTS to B and receiving from another node simultaneously, A will experience a collision if B sends the CTS right after receiving the RTS. Thus, A informs B using the Time to wait field that it needs to wait for a certain time before sending the CTS. The Gossip signaling field contains information about neighborhood receivers.

- *UVOC-MAC states of operation*

The state transition diagram in Fig. 5.3 provides a complete depiction of UVOC-MAC. In the Idle state, nodes simply decode received messages and update the corresponding tables. Upon receiving an RTS, a receiver checks the Time to wait field and sets a timer. It sends CTS upon timer reaching zero. The direction to send the CTS is determined by the Occupancy table. At this point, the node transits to the Receiving DATA state.

If a node has new data to send in Idle state, it runs the check table procedure and sends an RTS (directionally with the best available configuration) and transits state Wait for CTS. In this state, a node still decodes signals that it receives and update tables until it experiences a CTS timeout. If the node receives the expected CTS, it enters the state Sending DATA; if not, upon timeout, it transits into state Back off. When a node receives a CTS it checks the selected angle field to identify the direction of transmission and the corresponding rate. It then sends DATA directionally. While sending DATA, the node can receive other intended RTS messages depending on whether full-duplex communications are possible (the selected pointing angle is less than 40°). After having sent the DATA, the node stays in this state if it is still receiving from other nodes; otherwise it returns to the Idle state.

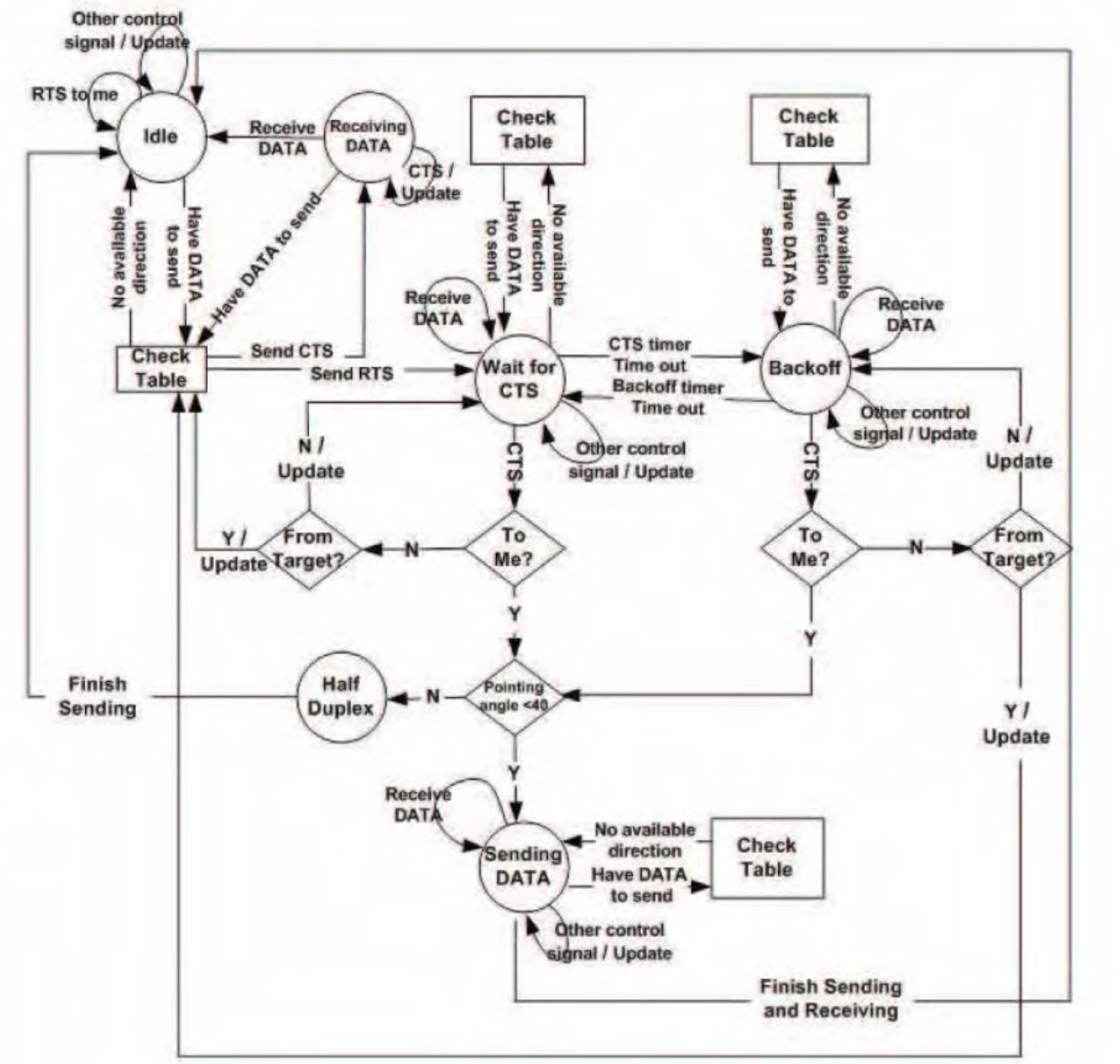

Figure 5.3: Detailed state transition diagram of UVOC-MAC.

5.1.3 Preliminary evaluation of UVOC-MAC

Handling problems with directionality: The use of an omni-directional CTS transmission alleviates the problem of hidden nodes and deafness to a large extent. However, a receiver may sometimes have to use a directional CTS transmission since otherwise, it interferes with an ongoing communication. In such cases, these problems can arise. Our gossip signaling successfully alleviates these problems to almost insignificant levels. The exposed node problem is not an issue with UVOC-MAC since in most cases, full-duplex communications are possible.

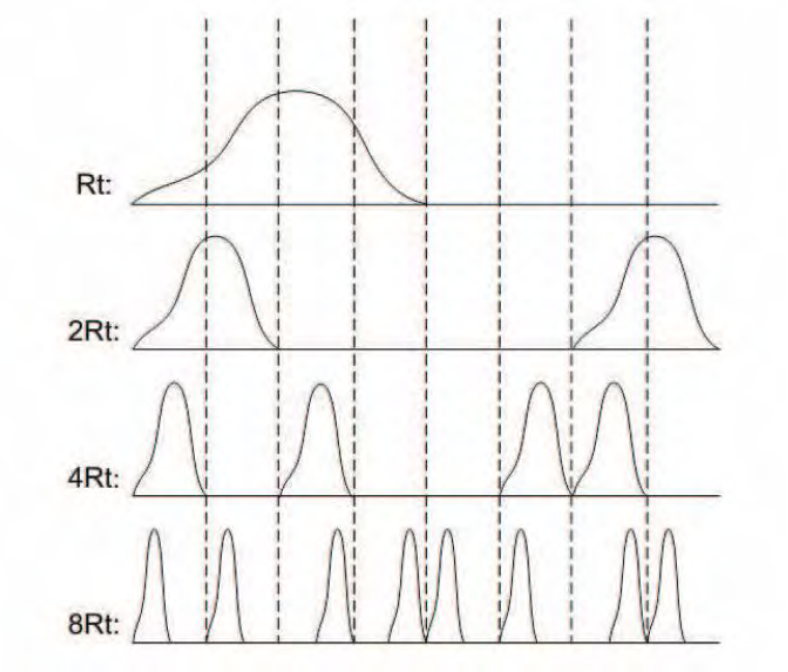

Figure 5.4: Dependencies between different data rates.

The use of multiple-transmission rates: UVOC-MAC is slotted and adaptively employs four data rates denoted by R_t, $2R_t$, $4R_t$, $8R_t$. The use of shorter pulse widths with PPM leads to higher data rates; recall that the choice of the pulse width is dictated by the delay spread which is in turn influenced by the pointing angle. The possibilities are shown in Fig. 5.4. A slot can accommodate two pulses. With binary PPM, a pulse in the first half of the slot (a sub-slot) indicates a '0' and a pulse in the second sub-slot indicates a '1'. From the figure we see that when a high rate projects interference on a low rate, there is practically no impact. This is because the energy-based detector simply computes the difference in the energy between the two sub-slots of a slot and in each lower rate sub-slot, a similar interference energy is added. Note here, those results are for a given distance. As an example, when an $8R_t$ rate transmission interferes with a $4R_t$ rate transmission, an interference pulse of identical magnitude is added to each sub-slot of the lower rate transmission. However, as one can immediately see, interference from lower rate transmissions impact higher rate transmissions. Thus, UVOC-MAC disallows lower rate transmissions if they project interference at the receiver of a higher rate transmission; it allows the initiation of lower rate transmissions as long as there is no such impact.

- *Analysis of collision probabilities*

Our goal in this section is to show that the collision probabilities in UVOC networks are high if no regulation is used (like with ALOHA) via a simple analysis. Let us assume that the distance between the intended transmitter and receiver is r_0 and the corresponding off-axis angle is ϕ_0. The interferer (say i) is located at distances r_i and has corresponding off-axis angle ϕ_i. We assume that interferers are uniformly distributed in the area with radius R centered at the intended receiver. The ϕ_i is uniformly distributed in $\{0, \pi\}$; the analysis can be easily modified for other distributions of r_i and ϕ_i.

We consider two popular models for characterizing a successful reception: (a) the protocol model and (b) the physical model. With the two models, a collision occurs if:

$$P(\text{collision})=\begin{cases} P(\max_k(p_k)\geq \frac{p_0}{T}) \text{(protocol model)} \\ P(\sum_{k=1}^{m} p_k \geq \frac{p_0}{T}) \quad \text{(physical model)} \end{cases}, \qquad (1)$$

where m is the total number of interfering nodes around the desired receiver; p_k is the received power from k^{th} interfering node; p_0 is the received power from the intended transmitter; T is the SINR threshold. Recall that with UVOC signal detection is typically energy-based. Thus, the additive interference model is a good fit. In other words, the physical model can capture the behaviors with UVOC better. However, the protocol model offers simplicity and hence we consider it as well. With the protocol model we only consider the interference from the strongest interferer; thus, the performance with this model is somewhat optimistic.

The received signal power is given by $p_0=p_t c r_0^{-a}\exp(-b\phi_0)$ and the interference power by $p_i=p_t c r_i^{-a}\exp(-b\phi_i)$. Here, the coefficient $c=1/\xi$. Let $z = r_i^{-a}\exp(-b\phi_i)$. The probability density function (PDF) of z can be easily computed given the PDFs of r_i and ϕ_i. The pdf of z is given by (we omit the derivation due to space constraints):

$$f(z)=\begin{cases} \frac{1}{zb\pi}-\frac{\exp(-2b\pi/a)}{b\pi R^2}\cdot z(-\frac{2}{a}-1) \quad (\frac{\exp(-b\pi)}{R^a}<z<\frac{1}{R^a}) \\ (\frac{1}{b\pi R^2}-\frac{\exp(-2b\pi/a)}{b\pi R^2})\cdot z(-\frac{2}{a}-1)(\frac{1}{R^a}<z<\xi) \end{cases}. \qquad (2)$$

Note here that path loss cannot be smaller than 1, z has an upper bound of ξ so that PDF of z needs normalization. We can then derive the probability that the interference power exceeds the desired threshold (as per the protocol model) to be:

$$P_C = P(p_i \geq \frac{p_0}{T}) = P(r_i^{-a}\exp(-b\phi_i) \geq \frac{r_0^{-a}\exp(-b\phi_0)}{T})$$

$$= P(z \geq \frac{r_0^{-a}\exp(-b\phi_0)}{T}) \qquad (3)$$

$$= \begin{cases} \frac{2a\ln\frac{r_0}{R}+2b\varphi_0+2\ln T+a}{2b\pi} - \frac{a}{2b\pi}\frac{r_0^2}{R^2}\exp(\frac{-2b\pi}{a})\exp(\frac{-2b\varphi_0}{a})T^{\frac{2}{a}} \\ \qquad \text{when } \frac{r_0^{-a}\exp(-b\varphi_0)}{T} \leq \frac{1}{R^a} \\ \frac{a}{2b\pi}\frac{r_0^2}{R^2}(1-\exp(\frac{-2b\pi}{a}))\exp(\frac{-2b\varphi_0}{a})T^{\frac{2}{a}} \\ \qquad \text{when } \frac{r_0^{-a}\exp(-b\varphi_0)}{T} > \frac{1}{R^a} \end{cases}.$$

The final expression is simply obtained by integrating f(z) over the desired interval. P_c is the probability that one of the interferers (say i) causes a collision at a particular target. With the protocol model, a collision occurs if at least one of these m interferers causes a collision. Thus,

$$P_{protocol}(\text{collision})=1-(1-P_c)^m. \qquad (4)$$

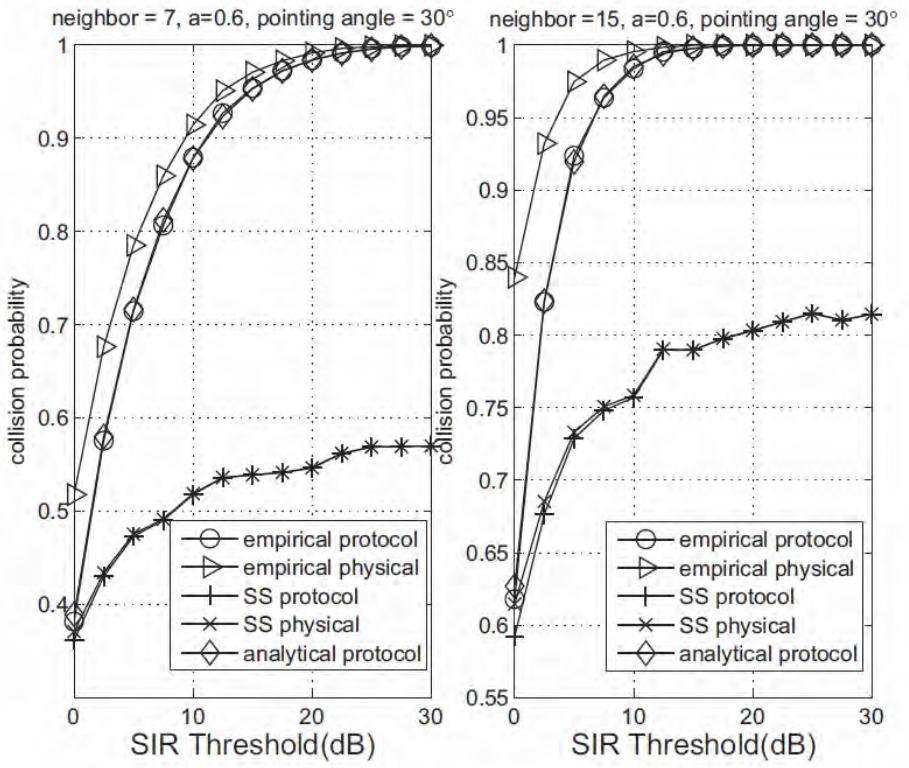

Figure 5.5: Collision probability for a given pair of nodes with distance r_0=67m and off-axis angle ϕ_0 =10° within the area R=100m; the pointing angle is 30°. Left figure shows the scenario with 7 interferers around and right figure with 15 interferers around.

Numerical results based on the above analysis are compared with Monte Carlo simulation results using the proposed non-coplanar path loss model (referred to as the empirical model) and the single scattering non-coplanar path loss model from [4]. With each, we consider both the protocol and physical collision models. r_0 and ϕ_0 are set to 67m and 10 °, respectively. r_i is distributed with probability density $2r/R^2$ in {0,100}m and ϕ_i is uniformly chosen from {0,180}° . Note here that the mean value of r_i is 67m; r_0 is chosen to be this value. The comparisons are presented in Fig. 5.5. We observe that the analytical results match the results from the Monte Carlo simulations using the empirical model quite well. This is expected since the analysis uses the same path loss model as that of the empirical model. However, since the channel attenuation is different with the SS model, the results differ.

Second, we observe that the larger the number of interfering nodes, the larger the discrepancy between the analytical protocol model and empirical physical model. This is because as the number of interferers increases, the protocol model (accounts for only one dominant interferer) becomes less and less accurate.

Third, the discrepancy between protocol and physical models with the SS path loss model, is negligible. This is because the SS model inherently assumes that received power is zero if the interfering node has no common volume with the target FOV. With this, the accumulated interference is very close to the maximum interference. Recall however, this model is inaccurate as we see in our experiments.

Fourth, the SS model yields smaller collision probabilities than the empirical non-coplanar model as the SINR threshold increases. This is because, the multiple scattering is captured by the empirical model and this accurately captures higher levels of interference thus, increased collision probabilities. In fact, due to this, the collision probability does not reach '1' for the range of SINR values considered.

5.1.4 Simulation results

In this section, we evaluate the performance of UVOC-MAC with OPNET version 16.0.

Simulation settings: The default simulation settings are listed in Table 5.1. The chosen transmission power corresponds to the typical short UV transmission range (approx. 100m). A packet generated by a node is targeted towards a randomly chosen neighbor. We use the channel attenuation and delay spread results from our PHY experiments to characterize signal propagation. All the path propagation parameters are consistent with that in the outdoor experimental settings. The nodes are randomly distributed in the deployment area (network size).

Table 5.1: Simulation settings

Transmission power	4mW (2mW for each LED)
# of directions	6
SINR threshold	10 dB
Collision model	Physical (accumulative) model
Traffic pattern	200 pkt/sec
Packet size	1024 bits/pkt (data portion)
Network size	100m by 100m
# of nodes	8
RTS length	76 bits (without gossip)
CTS length	80 bits (without gossip)
DATA head length	76 bits
Simulation time	20 seconds

1) Setting up and maintaining connection tables

Connection tables are assumed to be available upon neighbor discovery. There are two ways to rank the entries in Connection tables: high-rate based method and path-loss oriented method. With the former, ranks favor lower pointing angles (thus higher rates). The entries associated with pointing angle leading to half-duplex communications are always ranked lower than those with smaller pointing angles. With the path-loss oriented method, ranks are assigned as per the measured path loss. Configurations with smaller path loss are assigned higher ranks.

2) Comparison of high-rate based and path-loss oriented methods

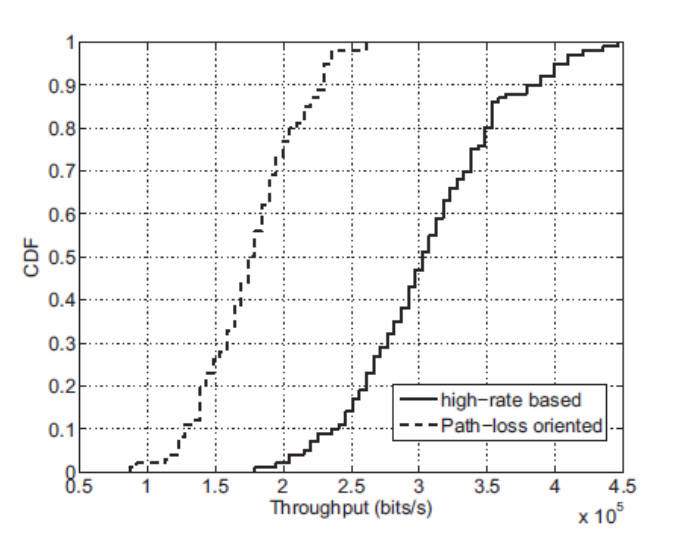

Figure 5.8: Throughput comparison with the two ranking methods.

With UVOC-MAC, we find that the above two maintenance methods result in different data rate usage distributions, throughput and collision probabilities. Naturally, the high-rate based method results in a more aggressive usage of high rates. The distributions with which the different data rates are used (from simulations) are shown in Table 5.2. We see that 93% of the transmissions are at rate $8R_t$. With the path-loss oriented method, in contrast, the rate $2R_t$ is used by about 90% of the transmissions. The latter effect is due to the fact that lower pointing angles result in higher path loss for a fixed off-axis angle; thus, a lower path loss typically corresponds to a higher pointing angle and thus a lower rate. Note here that in our simulations we find that the lowest rate is only scarcely chosen since it corresponds to a half-duplex mode with the lowest rank; almost always a higher rate is possible.

As seen from Fig. 5.8, the average throughput with the high-rate based method is about 74% higher than that with the path-loss oriented method. This is because higher rates directly lead to higher throughput.

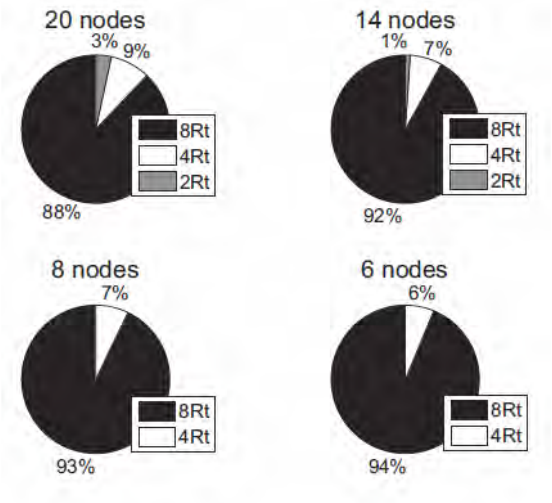

Figure 5.9: Usage of the different data rates with node density.

In Fig. 5.9, we depict the usage of the different rates with varying node densities. The high-rate based method is used. We observe that as the node density increases, there is an increased requirement towards using higher pointing angles and correspondingly lower rates. This is because, spatial reuse is more difficult if only the highest rate is used; the pointing angle dimension will have to be more heavily utilized in such cases (higher pointing angle).

3) Collision probabilities with UVOC-MAC

We observe the packets that are sent/received in a sample duration of 20 seconds. The results indicate that the collision probability (expressed as a percentage) is 19.83% with the high-rate based method while it is 23.61% when the path-loss oriented method is adopted. Note the drastic reductions that are achieved compared with 70.59% without UVOC-MAC (as discussed in Section
).

4) ACK transmissions

We observe from simulations that if we transmit ACKs at the base rate with UVOC, collisions might occur during the ACK exchange period. This is primarily because these low rate transmissions affect other high rate transmissions in the node's vicinity. Due to channel asymmetry, it is not a good idea for the receiver to send an ACK using received data rate. It is because in the ACK exchange, the receiver takes the role of the transmitter and the pointing angle and off-axis angles which are key in determining channel quality will have changed. Since nodes already have prior rough knowledge about communications in their neighborhood from updates, we seek to examine if ACKs are indeed needed. Unless stated otherwise, we perform simulation evaluations to understand if ACKs indeed help in improving throughput.

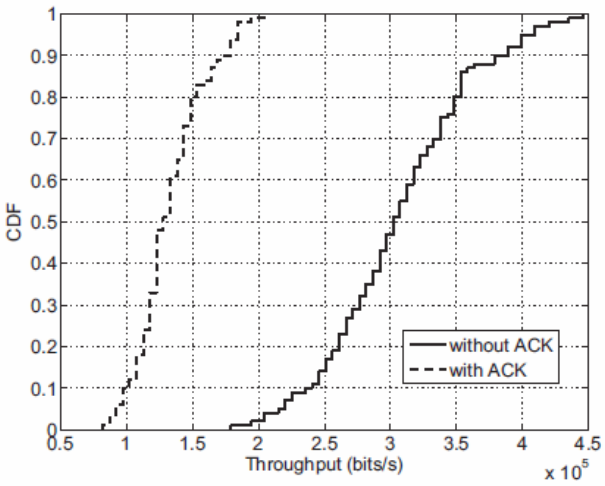

Figure 5.10: ACK impact on throughput.

Fig. 5.10 depicts the performance with or without the ACK process. We see that the ACK procedure brings down the throughput by about 132%; this loss is mainly due to the overhead and collisions with high rate transmissions. Also, as we indicted in the previous paragraph, the collision rate in the DATA part is very low (around 0.5%). Therefore, we conclude that it is better for UVOC to not include ACKs.

Table 5.2: Usage of different data rates

Rates	R_t	$2R_t$	$4R_t$	$8R_t$
High-rate based	0	0	7%	93%
Path-loss oriented	0	89.3%	4.9%	5.8%

5) Overhead in UVOC-MAC

The RTS-CTS handshake in UVOC-MAC allows nodes to update their tables. This padded information however inevitably introduces overhead. The overhead ratio is related to the packet size and can be calculated. For a packet size of 40k bits, the overhead ratio is only 1%.

$$\text{Overhead}=1-\frac{\text{Received DATA length (Pure DATA)}}{\text{Transmitted (RTS+CTS+DATA (total)) length}}.$$

6) Impact of tuning the pointing angle

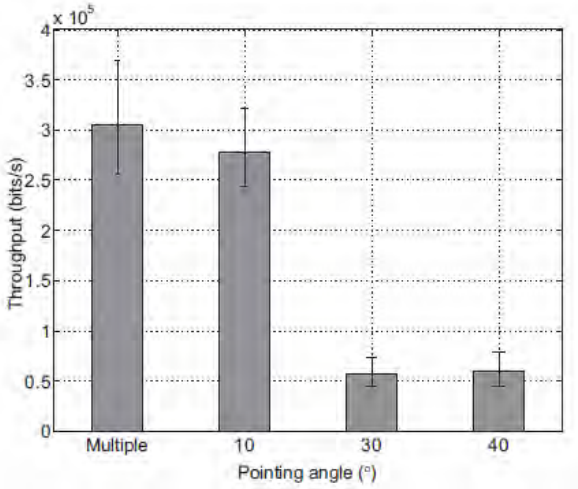

Figure 5.11: Impact of pointing angle on throughput.

One significant advantage of UVOC is the extra dimension of spatial reuse; as discussed this is exploited by varying the pointing angle. The additional spatial reuse from exploiting the pointing angle can be expected to lead to higher throughput. We conduct four sets of simulations to quantify the throughput improvements due to varying the pointing angle. The first set of simulations uses UVOC-MAC. In the other three sets, the pointing angles are fixed at 10°, 30° and 40°. Thus, adaptively in the additional dimension is eliminated. From Fig. 5.11, we see that the usage of multiple pointing angles brings about a 10% throughput increase compared to a case with a fixed 10° pointing angle. Compared with the other two cases, the throughput gains are much higher. The throughput is about 4.3 times that with fixed pointing angles of 30° or 40°. These results first demonstrate lower pointing angles are better (as one might expect). More importantly, if pointing angles were to be statically assigned, it may turn out that some pairs would have to use higher pointing angles (especially in dense scenarios). This would drastically hurt their throughput. UVOC-MAC provides adaptive tuning to opportunistically exploit the usage of lower pointing angles which in turn, improves throughput.

7) Exploiting full-duplex communications

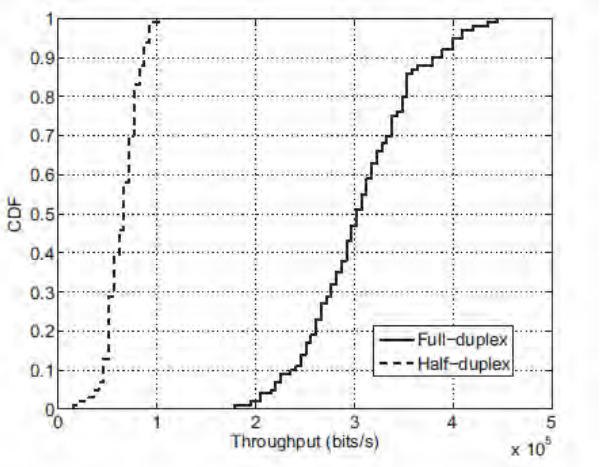

Figure 5.12: Throughput benefits of full-duplex communications.

Recall that UVOC nodes can communicate in full-duplex mode with small pointing angles. As discussed before, a conclusion drawn from the experiments was that pointing angles lower than 40° support full-duplex communications. We perform two sets of simulations to quantify the throughput gains from full-duplex opportunities with UVOC-MAC. In the first set, nodes can switch between half-duplex mode and full-duplex modes as per UVOC-MAC. In the other set, nodes operate in the traditional half-duplex mode. Fig. 5.12 depicts the throughput from the two sets. A 377.26% increase in throughput is brought by full-duplex opportunities. Again, note that in dense settings, if pointing angles were statically assigned, certain pairs may be forced to just operate in half-duplex modes and thus, achieve much lower throughput than what is possible with UVOC-MAC.

8) Impact of gossip signaling

If a node is in receiving state, it will most likely not be interfered with UVOC-MAC protection. But it will lose updates about ongoing communications in the network due to this kind of deafness. Gossip signaling increases the awareness with regard to ongoing communications in a node's neighborhood. This can significantly reduce unnecessary RTSs that would interrupt other transmissions and/or fail to establish connections. We evaluate the impact of gossip signaling in a 20-node topology. From the simulation results we observe that the gossip procedure reduces the number of RTS messages initiated by 32.3%. These are those RTS messages that did not result in a successful connection establishment.

9) Impact of system parameters

Finally, we examine the impact of various system parameters on the performance of UVOC-MAC.

Number of directions: Generally, the more the number of directions the better the spatial reuse. We find that UVOC-MAC effectively exploits an increase in the number of directions. From Fig. 5.13, we observe the throughput improves by 134.39% as the number of directions increases from 6 to 20.

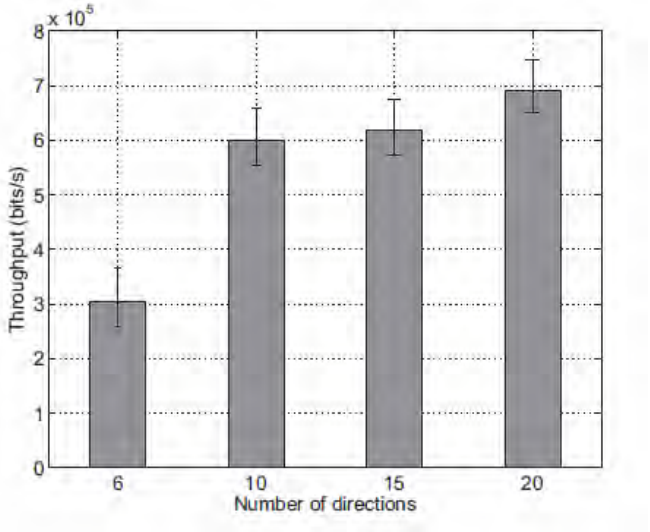

Figure 5.13: Throughput with different numbers of directions.

Packet size: Using longer packet sizes can potentially increase throughput due to decrease in the overhead per packet. However, it could also increase the collision probabilities. Fig. 5.14 shows the throughput trend with increasing packet size. To begin with, increasing packet size brings higher throughput. However, when the packet size increases to beyond a certain extent, the interference dominates and the throughput falls. The collision probability is 62.83% with 40k bits/packet compared with 19.83% for 1k bits/packet.

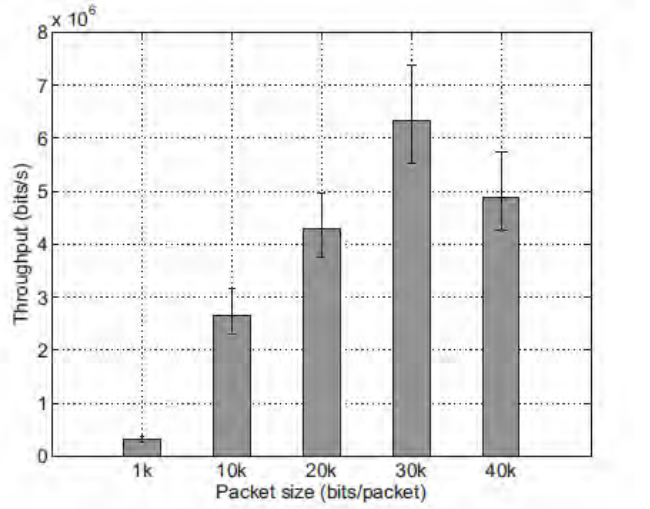

Figure 5.14: Throughput with different packet sizes.

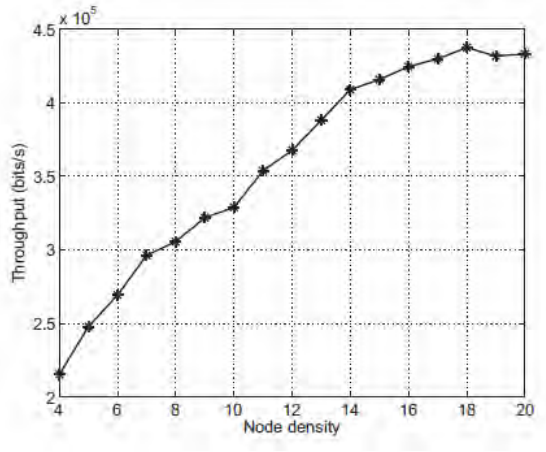

Figure 5.15: Throughput with different node densities.

Node density: To examine the impact of node density, we vary the number of nodes from 4 to 20. The nodes are uniformly distributed in a 100m by 100m area. Fig. 5.15 shows the network throughput versus node density. We see that the throughput is higher as node density increases. When the network is extremely dense (≈20 nodes) the throughput slightly decreases due to increased collisions. These results indicate that UVOC-MAC maintains high throughput even with high node densities.

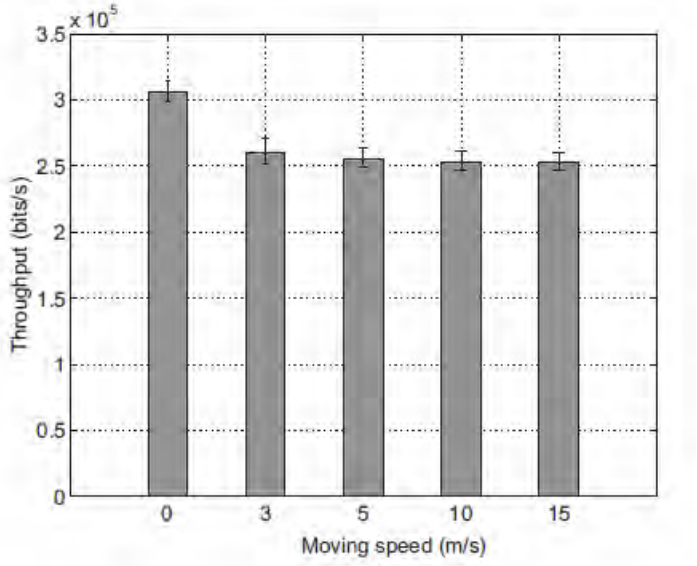

Figure 5.16: Throughput comparison at different moving speeds with a single moving node in network.

Impact of mobility: All above mentioned simulations are run in a static network. The connection tables are given and not changed in time. We want to examine how UVOC-MAC performs when the nodes are mobile. We expect these networks to be deployed in scenarios with pedestrian motion and thus, we consider low speeds. In Fig. 5.16, there is only one randomly chosen moving node and five different moving speeds are considered. We consider a random walk model where the node moves 1 m forward at each step; the rate at which it moves depends on the speed. The throughput decreases by 14.8% when the moving speed is 3 m/s. Higher speeds further bring reductions but the reduction is much smaller compared to that of the case when the speed changes from 0 m/s to 3 m/s. These reductions are because

the connections to moving node are sometimes expired (due to obsolete connection info) after it moves for certain time. We also check the performance when there are multiple nodes moving in the network. Fig. 5.17 shows the throughputs in four cases when one node, two, three or four nodes, respectively, are moving simultaneously. The moving speed for each node is 5 m/s and the moving direction for each node is chosen at random. From this figure, we see that the throughput decreases with an increase in the number of mobile nodes and the largest throughput reduction compared to static case is about 64.2%. We can conclude our UVOC-MAC is capable of tolerating minor changes of neighbor distribution. In order to be deployable in a fast-changing network, some neighbor maintenance techniques should be considered. We will examine this in future work.

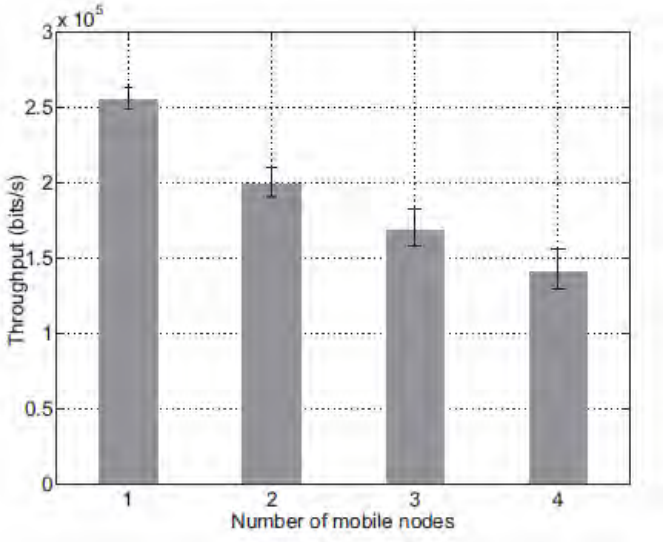

Figure 5.17: Throughput comparison with different numbers of moving nodes. Moving speed is 5 m/s.

UV MAC Summary

Communications with UV light is a good alternative to RF in many scenarios. Higher layer design for UV networks will have to conform to UV PHY properties. In this section, based on the understanding of the characteristics of UV PHY layer, we design UVOC-MAC, a MAC protocol that inherently accounts for the UV properties. We perform analysis and simulations to demonstrate that UVOC-MAC effectively exploits spatial reuse in extra dimensions. The throughput can improve by up to 4 times compared to a MAC that does not adaptively exploit the properties of the environment.

5.2 Neighbor discovery for UV network

Neighbor discovery schemes for UV communication: There have been a number of efforts on neighbor discovery for RF wireless networks assuming either directional or omni-directional antennas. Vasudevan et al. classify neighbor discovery algorithms into two categories: direct-discovery and gossip-based [48]. They analyze these two possibilities in synchronous and asynchronous scenarios and determine the frequency with which each node should send control packets to maximize the discovery probability within a certain time period. They find that the transmission probability is related to the number of neighbors and transmission beam width. The gossip-based algorithm outperforms the direct-discovery algorithm. Moreover, the performance of the gossip-based algorithm is not sensitive to the density of the

nodes. A handshake-based neighbor discovery algorithm is proposed with a time-division-multiple-access (TDMA) based media-access-control (MAC) protocol in 3D space in [49]. With an assumption that each node is equipped with GPS or inertial navigation system (INS), the authors suggest that the transmission power can be reduced to first find neighbors nearby and then increased gradually such that the probability of detection is increased. Luo et al. analyzed neighbor discovery in a code-division-multiple-access (CDMA)-like system and assumed each node is aware of its neighbors' names and signatures [50]. It is shown good performance is achieved by applying multiuser detection techniques; however, the assumptions are unrealistic for an ad hoc network. In [51], methods to save energy in neighbor discovery were researched and a flood-like procedure to achieve neighbor discovery was also suggested. Jakllari et al. proposed an integrated neighbor discovery and MAC protocol for ad hoc networks equipped with directional antennas [52]. The algorithm effectively utilizes directional antennas and accounts for the mobility of the nodes while performing neighbor discovery and maintenance. Vasudevan et al. comprehensively analyzed ALOHA-like neighbor discovery algorithms and proposed a collision detection mechanism to improve the performance in [53]. The algorithm enables each node to know when to terminate the neighbor discovery process without any a priori knowledge of neighbors.

Note that the above algorithms are not directly suitable for a UV ad hoc network. The unique UV scattering channel is fundamentally different from a RF channel. The scenarios are different from both directional and omni-directional antenna cases. The flexibility in both directional and omni-directional transmissions by a UV source (such as a UV LED) provides degrees of freedom in system design and operation that are not possible with RF. It is possible for a node to know not only the existence of the neighbors but also information about their locations without assistance of GPS or additional devices, contrary to most RF approaches. Thereby, we have to design a neighbor discovery scheme accounting for the unique characteristics of UV communications.

5.2.1 Credit-collection based neighbor discovery method for UVOC

For most military settings, the use of a centralized infrastructure is infeasible. Rapid reconfigurations and re-deployments are more the norm than the exception. Thus, ad hoc network deployments are typical in these contexts. Although there are some preliminary studies on medium access control, the network initialization process has not been considered before. This process is crucial for bootstrapping a network prior to operations. Since in typical cases, nodes are randomly deployed, each node will have to determine the existence as well as the locations of the surrounding nodes in order for information sharing. Thus, a distributed neighbor discovery algorithm is desirable for establishing connectivity and for self-organizing the network. Development of such algorithms is the focus of this work.

Each node in the network is assumed to be capable of directional transmissions and omni-directional receptions, given the unique properties of the UV channel. At the termination of neighbor discovery, a node in the network will have sufficient knowledge about each of its neighbors.

Based on the propagation properties we modeled and tested, we design our neighbor discovery mechanisms. First, we consider a well-planned deployment, wherein nodes are assigned a fixed set of synchronized directions in which they can point their beams. In other words, the sense of direction is global; when a node receives a message from a neighbor, it can immediately determine the direction in

which that neighbor transmitted its packet. We refer to this as neighbor discovery with direction synchronization. Second, we propose a more general neighbor discovery scheme, wherein nodes cannot determine a neighbor's direction by simply receiving the latter's transmission. The approach incorporates a novel handshake mechanism that is tightly dependent on the UV propagation characteristics [24].

- **Neighbor discovery with direction synchronization**

Since NLOS links are feasible for UV communications, we can expect that given several transmission directions from a remote node to the node of interest, more than one direction can be utilized for communication between this pair of nodes. Although the link loss varies significantly with pointing direction, all those links can function well if the background noise and multiuser interference are negligible. In practice, some small angles might not be feasible due to blockage by buildings, trees, vehicles, even people. However, some other directions resulting in links of degraded quality may still be usable. The neighbor discovery process should make all such link information accessible to neighbors. Each node must be made aware of the different NLOS links that it can use to its neighbors and the ranking of these links in terms of channel quality. It suffices if each node is made aware of the existence of its neighbors in a network with omni-directional antennas (as most prior efforts on neighbor discovery demonstrate). However, if directional antennas are utilized, a node needs to know the direction in which to send information to its neighbors. It is mentioned in [48] that GPS might be necessary or an angle-of-arrival (AOA) estimation technique must be applied to solve this problem. For many reasons including security, GPS might be unavailable in military contexts and low cost is preferable. We choose to develop an algorithm without a requirement for GPS. On the other hand, based on the energy detection and channel scattering characteristics of a UV communication system, AOA estimation is hard to implement. Thus, the issue of how to send information has to be solved by the neighbor discovery algorithm itself.

The neighbor discovery algorithm described in this section is specifically designed for a scenario with direction synchronization. Direction synchronization assumes that all the nodes in the network have the same number of fixed directions. The direction labeled "zero" in the direction table of each node should always reflect the same direction. With this assumption, once a receiver node, B receives a message sent by a transmitter node A, containing information with regards to the direction of node A's transmission, it can easily infer the best direction to reply to A, based on geometric symmetry (detailed discussion later). The reciprocal property of the channel is attributed to a homogeneous environment; the transmission pointing angles, the beam divergence angle and the FOV are set to be the same across all nodes. In this case, no handshake mechanism is necessary for direction synchronization. If the restriction of direction synchronization is relaxed, a feedback mechanism should be incorporated. We shall discuss such cases in the next section.

To rank each direction, intuitively, a receiver can record the received energy from a specific transmitter, from each direction. However, since we do not assume any multiuser detection technique, it is impossible to distinguish the desired signal from interference or background noise. We adopt a credit collection method to solve this problem.

- **Algorithm description**

The number and names of neighbors are unknown to the present node. The only information that the node has is the format of the transmitted message for the purposes of decoding. Only one type of message is transmitted in the network, i.e., the request packet which contains information of node identification (ID) and direction ID. Here, we require that each node has unique identification, which could be MAC address or any sequential code for node differentiation.

Every node sends out a request packet of duration of τ and receives all the time (due to the full-duplex capability). The interval between two successive transmissions follows exponential distribution with parameter λ. The node chooses the sending direction randomly.

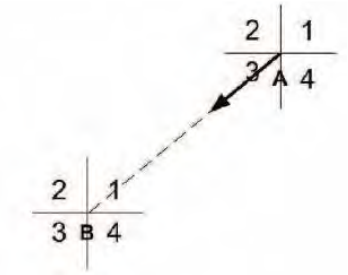

Figure 5.18: Illustration of direction synchronization.

Once a receiver node receives a request from another node, it extracts the information of source ID and the associated direction ID. Because all the nodes are assumed to be direction-synchronized, the receiver can figure out the direction in which it can respond to the transmitter. As shown in Fig.5.18, if node A transmits a request to node B using direction “3" and node B successfully receives A’s request, node B could conclude that its direction labeled “1" could be used to communicate with node A. Correspondingly, a reception from direction “2" suggests responses in direction “4", and vice versa. Since whether or not a node transmits is a random event, the total interference level the receiver experiences is a random variable. Thus, the successful reception of packets in a given direction follows a random process. Multiple transmissions of the same packet may lead to different outcomes; it may or may not be received depending on the interference levels from other nearby transmitters.

We collect the successfully received neighbor requests and create a credit table in which the directions of the successful requests are recorded. Each direction is then ranked as follows. A direction to a neighbor is assigned a credit upon correct detection of a packet from that direction. Each node transmits in a randomly chosen direction; the choice of direction is uniformly distributed. Packets sent from a better direction are deemed to be received with a higher possibility. Thus, for such directions the credits collected will be higher. Each node will then establish a ranked connection table for every neighbor after a sufficiently large number of transmissions are received, based on credit table. The more the packets are exchanged, the more reliable is the table. The steps of the process are formalized with the pseudo code below:

K = total no. of directions;

Clear credit table;

Transmitter:

```
if timer is up then
   ND request.source ID=self id;
   ND request.direc ID=uniformly choose(K);
   send ND request;
   set timer;
end if
Receiver:
if receive ND request then
   neighbor ID=ND request.source ID;
   prev direc=ND request.direc ID;
   current direc=[prev direc+ceil(K/2)] mod K;
   credit table.node[neighbor ID].direction[current direc]++;
end if
```

- **Simulation results**

Table 5.3: Simulation settings

Transmission power	4 mW
# of directions	6
SIR threshold	1 dB
Collision model	Physical (accumulative) model
Data rate	1 Mbps
Traffic pattern	10000 pkt/sec
Packet size	32 bits/pkt
Network size	100m by 100m
# of nodes	10

We study the neighbor discovery performance with direction synchronization, via simulations using OPNET version 16.0. The simulation settings are listed in Table 5.3. The chosen transmission power corresponds to the typical short UV transmission range (approx. 100m). We adopt the channel attenuation results from test to characterize signal propagation. The SIR threshold is set to 1dB, indicating that the signal is decodable if the signal power is slightly larger than the total interference power.

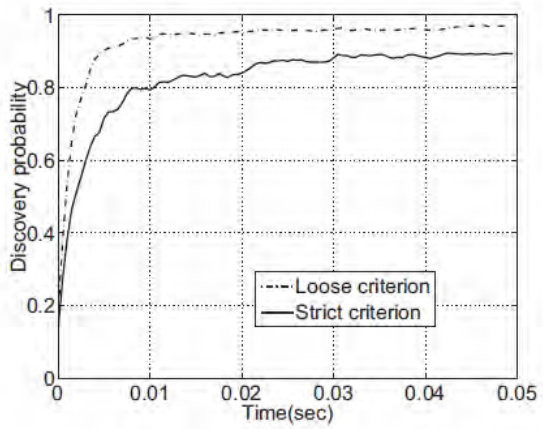

Figure 5.19: The discovery probability with loose and strict criteria.

In Fig.5.19, we consider two criteria for neighbor discovery. First, we impose a somewhat less stringent requirement (loose criterion) wherein a node seeks to establish only the top one third of all the directions to a neighbor; the ranking among these directions is inconsequential. For example, assume a node can perform transmissions in 6 directions, then we only focus on the top 2 directions between that node and any other node; the relative ordering of the two directions in terms of performance is not considered. We consider a direction to be correctly found if it is accurately classified as being or not being within the top one third of the possible directions.

Next, we consider a strict requirement (strict criterion) wherein, the relative ordering of the directions is necessary. In other words, the direction should be correctly classified in terms of its rank. In the solid curve, we consider the two top directions, now correctly ordered. In other words, a direction is considered to be found correctly if and only if it is exactly at the right position in the connection table.

It is observed that with the loose criterion, reaching a discovery probability of 90 % takes less than 0.005s, while the solid curve reaching the same probability takes about 0.05s. When there is a strict temporal constraint on the neighbor discovery process, the algorithms can still work well without providing poor directions (the top one third directions can be found) for communications among neighboring nodes.

We observe that while we can discover about 80 % of the directions with high accuracy relatively quickly, ordering among the top directions takes much longer (as evident from the figure). This is because, it is hard to distinguish between the top few directions; this is in some sense to advantageous since it becomes less important as to which direction is ranked higher.

Summary: In this section, we propose protocols for neighbor discovery in a UV ad hoc network. Due to the unique propagation properties of UV signal, each node may transmit or receive signals through NLOS links in different directions. A node should know the exact direction in which to transmit to its neighbors for best performance. Towards achieving this, our approach collects “credits" to rank all possible directions. We begin with basic algorithms with and without direction synchronization and then propose various techniques that can significantly enhance the performance of the neighbor discovery process. We perform extensive simulations to not only quantify the performance of our algorithms, but

also showcase the effects of various parameters such as the transmission power in use, and the random back-off times that node follow prior to sending neighbor discovery request or feedback packets.

5.2.2 Leadership based neighbor discovery method for UVOC

As may be evident from the previous description in previous section, a node needs to collect a sufficiently large number of credits in order to accurately rank the directions towards a given neighbor. Since the primary mode of communication is random access, collisions occur. This can skew the results small sample sets may not yield accurate estimates of the best direction. In other words, this results in short term inaccuracies. Convergence to correct results takes a relatively long period of time.

Given this limitation, and the importance of expeditious neighbor discovery, we seek to design an interference-free environment for the process. Our goal here is to enable the discovery of neighbors and the best direction for communications with each neighbor with a one-time packet exchange. We later show that our method (proposed below) drastically improves the performance of neighbor discovery in terms of the time taken [23], compared to the method proposed in section 5.2.1.

- **Our proposed approach:**

In a nutshell, our proposed approach relies on sequential neighbor discovery. A single node (the leader) initially performs neighbor discovery; after that node is done, the leadership is passed on to a second node and so no. We call our approach the “leadership-based neighbor discovery" protocol. In more detail, our approach consists of the following steps:

- Initially, all the nodes are in standby status. They only receive (listen) packets but do not transmit anything.
- A pre-chosen leader node (could be randomly chosen) will then initiiate the neighbor discovery process by sending a request packet in a randomly chosen direction. This request packet includes the ID of the sender and the direction in which it is transmitted.
- The leader waits for a fixed time period T, and then, switches to the next direction to send next request packet. It repeats the process until it performs packet transmissions in all possible directions.
- When a neighbor node receives a request packet from the leader node, it calculates the path loss experienced. Note that this is possible because there is no other concurrent transmission;(the path loss cannot be obtained since transmissions are subject to interference.)
- Each such neighbor waits for a period t; this period is randomly chosen in $[0,T]$. After this period, the neighbor randomly chooses a direction using which it transmits a feedback packet back to the leader. The feedback packet contains the ID of responding node and the path loss estimated using the request packet. The reception of the feedback packets is not guaranteed because contention exists among different neighbors that attempt sending feedback. However since contention is restricted to only the neighbors of the leader, it is likely to receive many of these feedback packets with a high probability.
- After the process is complete, the leader node can rank the directions for each discovered neighbor found based on the path loss information contained in feedback packets. It then randomly selects a successor from the nodes in its neighbor list. It sends a notifier packet to the selected successor node, using the best direction recorded for this node. The successor then performs neighbor discovery. All other nodes are made aware, that the neighbor discovery *token* has now been passed on to a different node.

It is possible that the notified packet gets lost; to account for this, if no request packets are heard from the successor for a period 2T, the former leader node will re-select a new successor. The process may have to be repeated in extreme cases until a successful leadership transfer is achieved. The steps described above are formalized with the pseudo code below:

```
K = total no. of directions;
Leader:
while rotation not finished yet do
if time T is up then
    ND request.source ID=self id;
    ND request.direc ID=uniformly choose(K);
    send ND request;
    set T;
else
  if receive ND feedback then
    neighbor ID=ND feedback.source ID;
    prev direc=ND feedback.prev direc;
    PathLoss=ND feedback.path loss;
    PathLoss.node[neighbor ID].direc[prev direc]=PathLoss;
     end if
   end if
end while
while i < # of neighbors do
    order PathLoss.node[i].direc[*];
end while
select leader=uniformly choose(# of neighbors);
send Notifier packet to next leader;
Other nodes:
if receive ND request then
    dest ID=ND request.source ID;
    prev direc=ND request.direc ID;
    PathLoss=Tx power/Rx power;
    set t=uniformaly choose(T);
    if time t is up then
        ND feedback.source ID=self id;
        ND feedback.prev direc=prev direc;
        ND feedback.path loss=PathLoss;
        send ND feedback;
```

end if

end if

- **Evaluations of our approach:**

Table 5.4: Parameters settings in simulations

Transmission power	4 mW
Number of directions	6
Transmission pointing angle	10°
SIR threshold	1 dB
Collision model	Physical (accumulative) model
Traffic pattern	10000 pkt/sec
Request packet size	32 bits/pkt
Feedback packet size	80 bits/pkt
Notifier packet size	32 bits/pkt
Network size	100m by 100m
Number of nodes	10

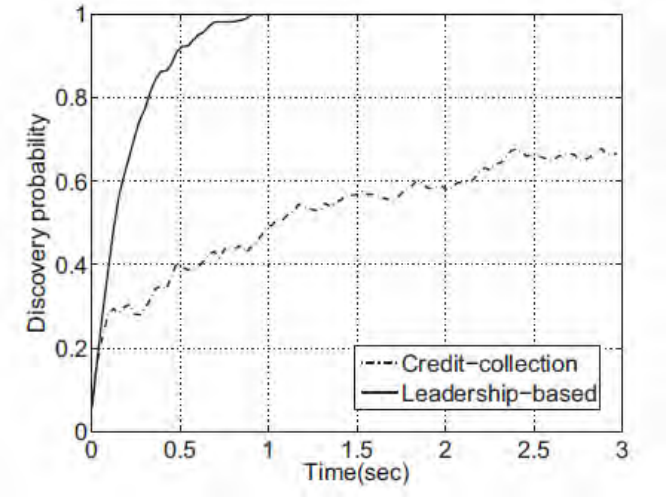

Figure 5.20: Comparison between leadership-based algorithm and credit-collection algorithm proposed

We evaluate the performance of our neighbor discovery protocol via extensive simulations performed using OPNET version 16.0. The simulation settings are listed in Table 5.4. The chosen transmission power corresponds to the UV transmission range (approx. 50m in Fig. 5.20). In all of the following simulations we assume that the transceiver has 6 directions for transmission operations. The more the directions, the larger the neighbor table maintained and the longer the neighbor discovery process takes. The relation between the number of directions and the time consumed by the neighbor discovery process is discussed later. We adopt the channel attenuation results from our test to characterize signal propagation. By default, the chosen parameters correspond to the scenario when the transmission pointing angle is equal to 10°. To recall, these parameters are: $\xi=5\times10^{9}$, $\alpha=0.4$, $b=8.7$. The SIR threshold is set to 1dB; the signal is detectable if the power is larger than the total interference power by this value.

The sizes chosen for the three kinds of packets are consistent with that with IEEE 802.11; we choose this since protocols for UV networks are yet to be standardized. Each node is placed randomly in a network area of $1\times10^4 m^2$. The total number of nodes in the network is 10. All the simulation curves are computed as averages of over 10 runs.

We compare the newly proposed protocol (labeled leadership-based) with the previously proposed protocol from section 5.2.1 (labeled credit-collection) in Fig. 5.20. We wish to point out here that this comparison is with the fastest version of the algorithm. The expected value of the waiting interval λ, for credit-collection is set to be 10^{-3}s. The uniformly distributed waiting interval T with the proposed protocol is set to be 2×10^{-3}s; this ensures that mean is 10^{-3}s and thus, the settings are consistent in both cases. In Fig. 5.20, we see the sharp speed up in the neighbor discovery process with the leadership-based approach. The leadership-based algorithm saves about 92% of the time consumed in neighbor discovery, if one were to have a requirement that every node find 70% of its neighbors in the network. It saves about 97% of the time consumed in neighbor discovery if this requirement is stricter and every node has to find about 80% of its neighbors. The credit collection protocol consumes a lot of time to stabilize. These results suggest that interference has a dominant influence on neighbor discovery in UV networks; using a relatively interference-free approach drastically speeds up the neighbor discovery process.

- **Improving fairness**

Although not explicitly stated earlier, we wish to point out here that a node can assume the role of the leader multiple times. We expect that the neighbor discovery process is a background process that is continuously executed; this is essential since the neighborhoods of nodes could change either due to failures, environmental changes (obstacles causing links to fail) or mobility. In this section, we consider the fairness of our approach in terms of the number of times a node gets an opportunity to being the leader.

Table 5.5: Records of being the leader (time length = 3 secs)

Find 100% neighbors					
Node ID	0	1	2	3	4
Leader counts	22	29	14	13	18
Node ID	5	6	7	8	9
Leader counts	21	22	18	12	25

To examine the fairness of our approach, we perform a simulation experiment wherein, we run the discovery process until all nodes discover almost all of their neighbors (> 99 %). The total simulation time was 3 seconds and node '0' was arbitrarily chosen to be the initial leader. Table 5.5 shows the number of times that each node is chosen to be the leader (referred to as leader records). We immediately see that certain nodes have a better chance at neighbor discovery; in other words, an imbalance is observed. Node 1 is chosen to be the leader 29 times; however, node 8 is only chosen 12 times. Table 5.6 shows the leader records up to the first 0.54 seconds of the simulation. In this period, the percentage of neighbors discovered is on average, 95% and 7 of the nodes had found all of their neighbors. We observe that node 0 and node 4 assumed the role of the leader 6 times each; many other nodes had the opportunity only twice. We also indicate in this table, the percentage of neighbors discovered within this time. We

observe that node 8 has discovered all of its neighbors even though it has been a leader just twice. Most nodes find all of their neighbors as long as they become a leader more than twice. This observation is encouraging in that, a node only has to serve as a leader a few times, in order for it to find its neighbors. If a node is chosen as a leader too often, it is likely to waste time and resources. Thus, it appears meaningful to provide equal opportunities of being a leader to all nodes in the network.

Table 5.6: Records of being the leader (time length = 0.54 secs)

Node ID	0	1	2	3	4
Leader counts	6	4	2	3	6
Neighbor percentage	1	1	0.75	0.89	1
Node ID	5	6	7	8	9
Leader counts	5	3	2	2	5
Neighbor percentage	1	1	0.81	1	1

- **Performance evaluation for improving fairness**

Figure 5.7 shows the percentage of neighbors discovered with time for a single realization from the perspective of an arbitrarily chosen node in the network. We simulate the 20 node scenario and other simulation settings are the same as described in previous section. In this figure, we see that the node under consideration found 35% of its neighbors after the first instance of being the leader; this percentage increased to 75% after its second instance of being the leader. However, as shown by the circle in the plot, after the node served as the leader for the third time, there was no new information obtained; note however that, the neighbor discovery was not complete for the node. Although the counter increased by 1, it was reset after the node served as a leader for the fourth time, since new information was acquired. The neighbor discovery procedure finally ended at 2.67 seconds because the counter threshold was reached. At that point, the node had indeed discovered all of its neighbors.

Table 5.7: Leader records after finding 100% neighbors

Node ID	0	1	2	3	4
Leader counts	6	4	5	7	4
Node ID	5	6	7	8	9
Leader counts	5	4	5	6	6
Node ID	10	11	12	13	14
Leader counts	5	6	6	4	2
Node ID	15	16	17	18	19
Leader counts	7	7	7	6	7

Table 5.7 shows the total leader counts after every node found 100% of its neighbors. We set the termination counter threshold mentioned above to be 2. Interestingly, from the Table 5.7 we observe that all the nodes except the one with node ID of 14 served as the leader without any information update, more than 2 times. This is because, node 14 was the final node in the neighbor discovery process; unless its counter was set to 2, the process could not be terminated. However, node 14 could be assigned to being a leader only by one of its neighbors. In this case, nodes attempted to search for 14 and interim also served as leaders again (the leadership token was passed around). Finally, the token was passed onto node 14 and the process terminated. Figure 5.21 shows the performance of the protocol with the termination procedure

with six scenarios, with different node densities. We see the termination time is proportional to the node density as one may expect.

Summary

Neighbor discovery in UV networks is an important function that allows nodes to bootstrap the topology and begin operations. While there have been a plethora of proposals for neighbor discovery in the RF context, they are inapplicable in the UV context given its unique PHY characteristics. In this chapter, we propose a novel neighbor discovery protocol for UV networks. The key idea is to eliminate interference by arbitrating the discovery process by using leaders; a leader is the only nodes that are allowed to perform neighbor discovery at any given time. The leadership role is passed on from node to node. We demonstrate that our protocol is extremely effective in performing neighbor discovery via extensive simulations that incorporate the UV PHY layer. In particular, the time needed for neighbor discovery process is decreased by as much as 90% as compared to the only previously proposed neighbor discovery scheme for UV networks. We also provide extensive evaluations to capture the impact of various network and system parameters on the performance of our protocol.

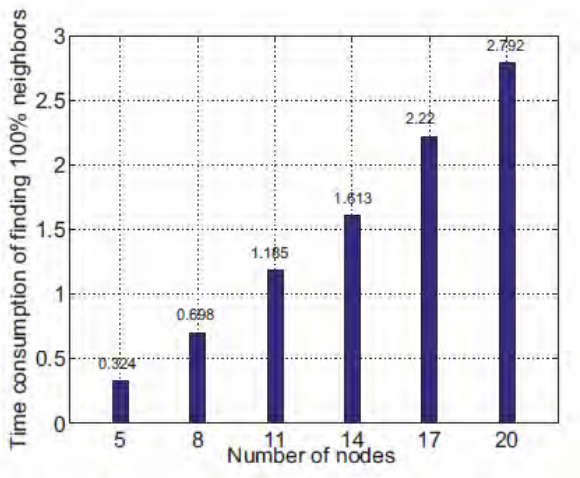

Figure 5.21: Illustration of the performance of the termination process with different node densities. All the nodes in the network find 100% of their neighbors.

6 Conclusions

This project explored multiple aspects of UV communication systems and networks, including channel modeling, system communication performance evaluation, network throughput, MAC protocol design and connectivity analysis.

In a NLOS UV communication network, UV signals suffer from huge extinction due to atmosphere absorption and scattering. In this project, first we focused on NLOS **UV scattering channel characterization and modeling**, especially NLOS UV channel impulse response and path loss modeling, and analyzed the UV link performance for short ranges. The single scattering and multiple scattering effects were included for cases of applicability. A NLOS UV single scattering channel model was parameterized and approximated for simplicity and tractability. Multiple scattering models were further analytically developed by simulating a complex process as a succession of elementary events whose probability laws were known. The closed-form expression of multiple scattering path loss enables easy study of higher order scattering effects. NLOS UV channel measurements were conducted extensively for varying geometries through our UV laser and LED-based measurement systems. Channel impulse response and path loss were measured and analyzed, providing a benchmark for theoretical and simulation results. Comparisons between experimental results and analytical models indicate that the single scattering assumption is adequate for short baseline range and small absorption and scattering coefficients. However, multiple scattering may dominate for large baseline ranges and dense atmosphere conditions. In addition, a gap appeared between measurements and analytical modeling for small pointing angles. The mismatch may be caused by measurement and other system errors, which is still under investigation.

Beside coplanar UV channel model, we also developed UV path loss models in non-coplanar geometry, analytically and empirically. The analytical model in the triple-integral form is a good candidate for link budget, and the closed-form analytical model developed greatly reduces the computation complexity and relaxes the constraint for the orientation of a receiver. The empirical **non-coplanar path loss model** provides a tool for system and network analysis thanks to its greatly simplified form. Meanwhile, the two analytical models are compared with a classic single scattering path loss model developed by Reilly et al and show a good match in most typical co-planar scenarios.

From the link modeling results, the UV communication performance was further predicted and evaluated. We demonstrated that a NLOS UV communication system is typically power limited rather than bandwidth limited even though significant pulse broadening exits after the channel. We also developed the model to account for the **scintillation effect for longer ranges**. Our case study showed a lognormal distribution for the received signal under turbulence. All of these modeling and analysis results can help to guide the communication system design and development of communication techniques.

Secondly, after the UV channel is clear, we explore the **communication performance limits** of outdoor UV links. Two typical phenomena, namely, the scattering effect and turbulence are investigated. The uniqueness in UV communications lies in the NLOS propagation path and ultra-low background

noise, which motivate the applications of a short range, loosely aligned optical link for wireless sensor or ad-hoc network. As a wireless UV link, the challenges arising from several sources. Firstly the scattering results in a huge path loss which limits the achievable range of NLOS UV communication. The multiple paths are also caused by the scatters in the atmosphere such that ISI effect can no longer be ignored for higher rates by introduced interference from neighboring symbols. Another obstacle to the implementation of a UV link can be the fading effect on the received signal since the wave front is distorted and the intensity fluctuates due to turbulence. Lastly device itself may not behave consistently well, the randomness of which has to be properly addressed in the design of an optical receiver. Our research aims to address above issues through theoretical modeling, experimental characterization and numerical analysis.

We characterized the tradeoffs between range and rate for an NLOS UV communication link through the abstraction in a Poisson photon counting model of IM/DD. The analysis incorporates the empirical path loss model of NLOS UV into the error probability derivation, Insights are gained towards how to plan the link budget. Generally speaking, PPM based modulation excels OOK in terms of achievable performance and synchronization. High elevation angles in geometry cause huge path loss such that the signal is attenuated enormously, which demands the adoption of a highly sensitive PMT to enable communication. To relax the stringent requirements on both a source and a receiver, the concept of NLOS relayed UV link has been proposed. The issue of directional interference is identified and a spatial reuse/time multiplex based MAC layer protocol has been introduced. Numerical results show the potential of such a scheme.

In this project, we analyzed the performance of LED-based ultraviolet communication M-PPM receiver in delay spread channel. Due to the relatively wide transmission beam angle of commercially available ultraviolet LED and scattering based propagation, inter-symbol interference introduced by channel spread is not negligible. Its effect becomes pronounced at a high data rate. However, most of the previous studies ignore the effect of inter-symbol interference. The results for the M-PPM receiver performance show the interaction among data rate, bit error rate and transmit/receive geometry.

The research further extended a point-to-point scenario to a **multiple user case**, and a UV communication network. A metric, transmission throughput, was designed to evaluate performance of an ultraviolet wireless network consisting of multiple nodes. The study incorporated newly proposed empirical path loss model and stochastic geometry theory. The lower bound of the transmission throughput was shown to be a function of node spatial density, transmission probability and signal detection threshold. Thus we are able to evaluate how these network parameters affect the network performance.

Higher layer design for UV networks has been studied in this research. The MAC schemes will have to conform to UV PHY properties. We first perform extensive experiments to understand and characterize the UV PHY layer. Then, we design UVOC-MAC, a MAC protocol that inherently accounts for the UV properties. This MAC scheme is suitable for full-duplex, four dimensional spatial reuse and multiple data rate adaptation. To study the performance of UVOC-MAC, we also provided collision probability

analysis and network simulations. Results show that UVOC-MAC brings reduced collision and enhanced throughput.

To construct and maintain a network, **neighbor discovery** is an essential process. Since UV communication is mostly attractive in military usage, the current neighbor discovery methods are not appropriate. Therefore, we propose protocols for neighbor discovery in a **UV ad hoc network**. We begin with basic algorithms with and without direction synchronization and then propose various techniques that can significantly enhance the performance of the neighbor discovery process.

In order to accelerate the network establishment, we propose a **leadership based neighbor discovery** protocol for UV networks. This algorithm drastically reduce the time required by neighbor discovery procedure by creating an interference-free broadcast environment. The nodes are able to terminate the neighbor discovery process as well.

We fully analyzed the connectivity issues of ultraviolet communication networks in different scenarios, i.e., different transceiver structures, depending on whether each node transmitter is capable of adjusting its pointing angle and tracking a target receiver. The research is the first work to analyze every aspect of multiple user ultraviolet communication networks.

Bibliography

[1] Z. Xu, H. Ding, B. M. Sadler, and G. Chen,"Analytical performance study of solar blind non-line-of-sight ultraviolet short-range communication links," Optics Letters, vol. 33, no. 16, pp. 1860-1862, Aug. 2008.

[2] Junge D M 1977 "Non-Line-of-Sight Electro-optic Laser Communications in the Middle Ultraviolet" (Monterey: Naval Postgraduate School)

[3] Ding H, Chen G, Majumdar A K and Xu Z "A parametric single scattering channel model for non-line-of-sight ultraviolet communications" Proc SPIE, E 7091 70910M 2008

[4] Wang L, Xu Z and Sadler B M "Non-line-of-sight ultraviolet link loss in noncoplanar geometry" Opt. Lett. 35 1263–5, 2008

[5] Wang L, Xu Z and Sadler B M "An approximate closed-form link loss model for non-line-of-sight ultraviolet communication in noncoplanar geometry" Opt. Lett. 36 1224–6, 2011

[6] Ding H, Chen G, Majumdar A K, Sadler B M and Xu Z "Non-line-of-sight ultraviolet communication channel characterization: modeling and validation" Proc. SPIE 7464 74640I 2009

[7] Ding H, Chen G, Majumdar A K, Sadler B M and Xu Z "Modeling of non-line-of-sight ultraviolet scattering channels for communication" IEEE J. Sel. Areas Commun. 27 1535–44, 2009

[8] Ding H, Xu Z and Sadler B M "A path loss model for non-line-of-sight ultraviolet multiple scattering channels" EURASIP J. Wireless Commun. Netw. 598572 2010

[9] G. Chen, F. Abou-Galala, Z. Xu, and B. M. Sadler, "Experimental evaluation of LED-based solar blind NLOS communication links," Opt. Exp., vol. 16, no. 19, pp. 15059–15068, Sept. 2008.

[10] G. Chen, Z. Xu, H. Ding, and B. M. Sadler, "Path loss modeling and performance trade-off study for short-range non-line-of-sight ultraviolet communications," Opt. Exp., vol. 17, no. 5, pp. 3929–3940, March 2009.

[11] Chen G, Xu Z and Sadler B M "Experimental demonstration of non-line-of-sight ultraviolet communication channel characteristics" Proc. SPIE 7814 781407 2010

[12] G. Chen, Z. Xu, and B. M. Sadler, "Experimental demonstration of ultraviolet pulse broadening in short-range non-line-of-sight communication channels," Opt. Exp., vol. 18, no. 10, pp. 10500–10509, May 2010.

[13] Chen G, Drost R J, Sadler B M and Liao L “Long-distance ultraviolet scattering channel measurements: analog versus digital approaches” Conf. on Lasers and Electro-Optics JTu4A. 88 2013
[14] Gang chen, Linchao Liao, Zening Li, R. Drost and B. Sadler.“Experimental and simulated evaluation of long distance NLOS UV communication” In CSNDSP, Manchester, UK, 2014
[15] M. R. Luettgen, J. H. Shapiro, and D. M. Reilly,“Non-line-of-sight single-scatter propagation model,” J. Opt. Soc. Am., vol. 8, no. 2, pp. 1964-1972, Dec. 1991.
[16] Ding,H, Chen,G,Xu,Z and Sadler B.M, “Channel modelling and performance of non-line-of sight ultraviolet scattering communications”, IET Communications, 6(5),514-524(2012)
[17] H. Ding, G. Chen, A. K. Majumdar, B. M. Sadler, and Z. Xu, “Turbulence modeling for non-line-of-sight ultraviolet scattering channels,” in Proc. SPIE, vol. 8038, 2011, 80380J.
[18] Linchao Liao, Gang Chen, Brain M. Sadler, “GPS synchronized UV communication system performance based on USRP”, SPIE Photonics and Optics, Laser Communication and Propagation through the Atmosphere and Oceans, San Diego, CA, August 25-29, 2013.
[19] H. Ding, G. Chen, Z. Xu, and B. M. Sadler, "Characterization and modeling of non-line-of-sight ultraviolet scattering communication channels,” IET Communications Special Issue on Photonic and Free Space Optics Networks, IET Commun., 2012, Vol. 6, Iss. 5, pp. 514–524.
[20] H. Ding, G. Chen, A. Majumdar, B. M. Sadler, and Z. Xu, “Turbulence modeling for non-line-of-sight ultraviolet scattering channels," Proc. of SPIE Photonics and Optics - Atmospheric Propagation VIII, Florida, FL, April, 2011 (Invited).
[21] Y. Li, J. Ning, Z. Xu, S. V. Krishnamurthy, and G. Chen, “UVOC-MAC: A MAC Protocol for Outdoor Ultraviolet Networks.” IEEE, 2010.
[22] Z. Xu, G. Chen, F. Abou-Galala, and M. Leonardi, "Experimental performance evaluation of non-line-of-sight ultraviolet communication systems," Proc. of SPIE Photonics and Optics - Free Space Laser Communications VII, Vol. 6709, San Diego, CA, August 28-30, 2007.
[23] L. Wang, Y. Li, Z. Xu, S. V. Krishnamurthy, “A Novel Neighbor Discovery Protocol for Ultraviolet Wireless Networks,” MSWiM’11, October 31–November 4, 2011, Miami, Florida, USA.
[24] Y. Li, L. Wang, Z. Xu, and S. V. Krishnamurthy, “Neighbor Discovery for Ultraviolet Ad Hoc Networks”, IEEE Journal on Selected Areas in Communications, Volume 29 (10), Dec. 2011.
[25] L. Wang, Y. Li, and Z. Xu, “On connectivity of wireless ultraviolet networks”, JOSA A, Vol. 28, Issue 10, pp. 1970-1978, 2011.
[26] Q. Gao and G. Chen, “Non-line-of-sight Ultraviolet Communication Based on DHT ACO-OFDM”, Proc. of SPIE Photonics and Optics, Laser Communication and Propagation through the Atmosphere and Oceans, Vol. 8517, San Diego, CA, August 12-16, 2012.
[27] Larry C. Andrews; Ronald L. Phillips, "Laser Beam Propagation through Random Media, Second Edition," vol. PM152, pp. 442-427, Sep, 2005.
[28] R. M. Gagliardi and S. Karp. Optical Communications 2nd Ed. John Wiley and Sons, Inc, New York, 1995.
[29] John G Proakis. Digital Communications 3rd Ed. McGraw Hill, New York, 1995.
[30] O. Oyman, N.J. Laneman, and S. Sandhu. Multihop relaying for broadband wire¬less mesh networks: From theory to practice. IEEE Communications Magazine, 45(11):116 -122, november 2007.
[31] M. Safari and M. Uysal. Relay-assisted free-space optical communication. IEEE Transactions on Wireless Communications, 7(12):5441 -5449, december 2008.
[32] T. A. Tsiftsis, H. G. Sandalidis, G. K. Karagiannidis, and N. C. Sagias. Multihop free-space optical communications over strong turbulence channels. In IEEE In¬ternational Conference on Communications, 2006. ICC，06. Volume 6, pages 2755 -2759, june 2006.
[33] Q He, B. M. Sadler, and Z Xu. Modulation and coding tradeoffs for non-line-of-sight ultraviolet communications. Proc. SPIE, 2009.

[34] Q He, B. M. Sadler, and Z Xu. On the achievable performance of non-line-of-sight ultraviolet communications. Proc. OSA, 2010.
[35] Q. He and Z. Xu. Opportunistic cooperation for fso links aided by decode and forward relay. In Accepted by IEEE Globecom Workshops (GC Wkshps), 2012, pages 1015 -1019, Dec. 2012.
[36] Q. He and Z. Xu. Outage analysis of opportunistic cooperation for fso communi¬cation links. Submitted to Journal of Lightwave Technology, 2012.
[37] Q. He, Z. Xu, and B. M. Sadler. Non-line-of-sight serial relayed link for optical wireless communications. In IEEE Military Communications Conference, 2010 - IEEE Milcom 2010, pages 1588 -1593, 31 2010 Nov. 3 2010.
[38] Q. He, Z. Xu, and B. M. Sadler. Performance of short-range non-line-of-sight led- based ultraviolet communication receivers. Opt. Expr., 18(12):12226-12238, 2010.
[39] G. Prati and R. Gagliardi. Block encoding and decoding for the optical ppm channel (corresp.). IEEE Transactions on Information Theory, 28(1):100 - 105, jan 1982.
[40] R.R. Choudhury, X. Yang, R. Ramanathan, and N.H. Vaidya. Using directional antennas for medium access control in ad hoc networks. In ACM MobiCom, September 2002.
[41] R.R. Choudhury and N.H. Vaidya. Deafness: A MAC problem in ad hoc netwroks when using directional antennas. In IEEE ICNP, October 2004.
[42] A. Nasipuri, S. Ye, J. You, and R.E. Hiromoto. A MAC protocol for mobile ad hoc networks using directional antennas. IEEE WCNC, September 2000.
[43] C.M. Cordeiro, H. Gossain, and D.P. Agrawal. A directional antenna medium access control protocol for wireless ad hoc networks. In Brazilian Telecommunication Society, 2005.
[44] T. Korakis, G. Jakllari, and L. Tassiulas. A MAC protocol for full exploitation of directional antennas in ad-hoc wireless networks. In MobiHoc, 2003.
[45] J. Wang, Y. Fang, and D. Wu. SYN-DMAC: A directional MAC protocol for ad hoc networks with synchronization. In MILCOM, 2005.
[46] H. Gossain, C. Cordeiro, and D.P. Agrawal. MDA: An efficient directional MAC scheme for wireless ad hoc networks. In GLOBECOM, 2005.
[47] M. Takata, M. Bandai, and T. Watanabe. A directional MAC protocol with deafness avoidance in ad hoc networks. IEICE trans on Communications, E90-B(4), 2007.
[48] S. Vasudevan, J. Kurose, and D. Towsley. On neighbor discovery in wireless networks with directional antennas. In IEEE INFOCOM, March 2005.
[49] G. Pei, M. Albuquerque, J. Kim, D. Nast, and P. Norris. A neighbor discovery protocol for directional antenna networks. In MILCOM, October 2005.
[50] J. Luo and D. Guo. newblock Neighbor discovery in wireless ad hoc networks based on group testing. In 46th Annual Alerton Conference, September 2008.
[51] M.J. McGlynn and S.A. Borbash. Birthday protocols for low energy deployment and flexible neighbor discovery in ad hoc wireless networks. In Mobihoc, September 2001.
[52] G. Jakllari, W. Luo, and S.V. Krishnamurthy. An integrated neighbor discovery and MAC protocol for ad hoc networks using directional antennas. IEEE trans on wireless communications, 6(3), 2007.
[53] S. Vasudevan, D. Towsley, R. Khalili, and D. Goeckel. Neighbor discovery in wireless networks and the coupon collector's problem. In ACM Mobicom, 2009.